# Calculations on the two-point function of the $O(N)$ model

Federico Benitez*
*Instituto de Física, Facultad de Ciencias, Universidad de la República, Iguá 4225, 11000 Montevideo, Uruguay*

Ramón Méndez-Galain† and Nicolás Wschebor‡
*Instituto de Física, Facultad de Ingeniería, Universidad de la República, J.H.y Reissig 565, 11000 Montevideo, Uruguay*
(Received 24 October 2007; published 31 January 2008)

The self-energy of the critical three-dimensional $O(N)$ model is calculated. The analysis is performed in the context of the nonperturbative renormalization group by exploiting an approximation which takes into account contributions of an infinite number of vertices. A very simple calculation yields the two-point function in the whole range of momenta, from the UV Gaussian regime to the scaling one. Results are in good agreement with best estimates in the literature for any value of $N$ in all momenta regimes. This encourages the use of this simple approximation procedure to calculate correlation functions at finite momenta in other physical situations.

DOI: 10.1103/PhysRevB.77.024431 PACS number(s): 03.75.Hh, 05.30.Jp

## I. INTRODUCTION

The $O(N)$ scalar model describes many phenomena in a wide range of physical situations. Besides the $N=1$ case, which corresponds to Ising-like systems, with a wide range of applications as, e.g., liquid-gas transition, the $N=2$ model describes superfluid helium, $N=3$ can be used to study ferromagnets, $N=4$ allows the study of the Higgs sector of the standard model at finite temperature, and the $N=0$ case describes the physics of some polymers.[1] As a natural consequence, a huge amount of work has been devoted to the study of this family of models. Leaving aside the $d=2$ case, where specific methods exist, most of the existing results correspond to thermodynamical properties, as critical exponents or phase diagrams, i.e., physical quantities encoded in correlators at small external momenta, e.g., the effective potential. With this goal, very complicated techniques, such as resummed perturbative calculations carried up to seventh order,[1,2] high-temperature expansions,[3–5] or Monte Carlo methods,[4–8] were used. When instead trying to get physical quantities depending on finite momenta, such as the self-energy of the model, fewer results can be found in the literature (see, for example, Ref. 9 and references therein). All these calculations suffer from a common difficulty, which is general to a vast class of problems: It is extremely nontrivial to deal with systems having highly correlated components. In this sense, as the $O(N)$ model is simpler than most other such problems, it has been largely used as a testing ground for the development of calculation schemes in nonperturbative contexts.

The nonperturbative renormalization group[10–14] (NPRG) is a general framework conceived to deal with this kind of situations. It is based in an infinite set of exact equations giving all renormalized correlation functions between the various components of a given system. Naturally, as one has to deal with an infinite tower of coupled differential equations, in order to solve them, the use of approximations is unavoidable. Several years ago, a systematic approximation scheme was developed[14–16] which allows for the solution of this set of equations in a particular case: The so-called derivative expansion (DE) is based in an expansion in the powers of the derivatives of the fields. Even if there is no formal proof of its convergence, the DE has provided very competitive results in problems where only small (eventually zero) external momenta play a role. Among many other applications (see, e.g., Refs. 16–18), the approximation was applied to the $O(N)$ model,[16,19–23] even up to the next-next-to-leading order of the scheme in the $N=1$ Ising case,[24] yielding at this order critical exponents of a similar quality as those obtained using seven-loop resummed perturbative calculations.

On the other hand, when trying to describe phenomena involving all modes, the situation is different. For example, to get the transition temperature of a dilute gas to a Bose-Einstein condensate, one needs the self-energy of the $O(2)$ model in three-dimensions at arbitrary momenta;[25] relevant information comes from the intermediate momentum region between the IR and the UV ranges. Within the NPRG, only calculations including a finite number of vertices[26] had been considered up to now, either in $O(N)$ (Refs. 27–31) or in more involved problems such as QCD.[32,33]

Recently, a general approximation scheme suitable to get any $n$-point function at any finite momenta within the NPRG has been proposed.[34] The strategy has many interesting similarities with DE. First, it can be applied, in principle, to any model. Second, although the approximation is not controlled by a small parameter, it can be systematically improved. Furthermore, this strategy reproduces both perturbative and DE results, in their corresponding limits; for example, if solving the two-point function flow equation at the leading order (LO) of the procedure, the two-point function includes all one-loop contributions while the effective potential includes all two-loop ones. It is possible to apply, on top of the approximation presented in Ref. 34, an expansion in powers of the field, as frequently done in DE; at least in the studied case, this expansion seems to converge rapidly.[35] Nevertheless, when considering only the first order of the expansion, the correct result for a quantity such as the critical exponent $\eta$ can be missed by as much as 60%. Thus, as an expansion in powers of the field corresponds to an expansion in the number of vertices,[35] the latter remark is a strong support to

 

approximations, as that of Ref. 34, which simultaneously include an infinite number of vertices.

The LO of the procedure was used in Ref. 36 in order to calculate the two-point function of the $N=1$ case. Following a simple (and yet accurate) strategy, it was shown that, within an analytical and numerical effort similar to that of the DE, one gets a self-energy with the correct shape at all momentum regimes. One gets the logarithmic UV behavior; its precoefficient, which is in fact a two-loop quantity, follows with only 8% error. In the IR, critical exponents are obtained with a quality similar to that of DE at next-to-leading order (NLO). As for the intermediate crossover regime, a quantity sensitive to this range of momenta was calculated to get a result close to the error bars of both lattice and resummed seven-loop calculations.

The purpose of this paper is to apply the method presented in Ref. 34, at its LO, to the $O(N)$ model. In Ref. 34, it was shown that the LO of the procedure is already exact in the large $N$ limit of the model. Moreover, in this limit, a simple analytical solution of the $n$-point functions at finite momenta was presented. Here, we shall implement the method, at any value of $N$, in order to numerically solve the approximate flow equations of the two-point function at criticality and in $d=3$. We shall follow a simple strategy, similar as that used in Ref. 36.

The paper is organized as follows. In the next section, we shall present the general approximation procedure introduced in Ref. 34 in the framework of a field theory with $N$ boson fields and, in particular, when the model has $O(N)$ symmetry. In Sec. III, we shall present two possible strategies to solve the two-point function equations: the first one is simpler, but it loses the above mentioned two-loop exactness of the effective potential, and in the second strategy, with a slight increase in the numerical effort, the two-loop exactness is recovered. In Sec. IV, we present our results, both in the scaling sector and at large and intermediate momenta; in particular, we calculate some quantities to gauge the quality of the two-point function thus obtained and compare our results with those following from other means. Finally, in Sec. V, we study analytically the large $N$ behavior of our results, both at leading and next-to-leading order in $1/N$ and compare them with numerical results of the previous section, as well as with exact results known in the literature.

## II. APPROXIMATION SCHEME

In this section, we shall briefly present the general formalism of the NPRG and describe the approximation scheme to calculate $n$-point functions at finite momenta introduced in Ref. 34. We shall make the presentation considering in the first place a generic Euclidean field theory with $N$ boson fields $\varphi_i$, denoted collectively by $\varphi$, with action $S[\varphi]$. Then, we shall specialize to the case where $S[\varphi]$ has an $O(N)$ symmetry.

The NPRG equations relate the bare action to the full effective action. This relation is obtained by controlling the magnitude of long wavelength field fluctuations with the help of an infrared cutoff, which is implemented[12–14,37] by adding to the bare action $S[\varphi]$ a regulator of the form

$$\Delta S_\kappa[\varphi] = \frac{1}{2}\int \frac{d^dq}{(2\pi)^d}(R_\kappa)_{ij}(q)\varphi_i(q)\varphi_j(-q), \tag{1}$$

where $(R_\kappa)_{ij}(q)$ denotes a family of "cutoff functions" depending on a parameter $\kappa$; above, a sum over repeated indices is understood. The role of $\Delta S_\kappa$ is to suppress the fluctuations with momenta $q \lesssim \kappa$ while leaving unaffected the modes with $q \gtrsim \kappa$. Thus, typically, $(R_\kappa)_{ij}(q) \sim \kappa^2 \delta_{ij}$ when $q \ll \kappa$ and $(R_\kappa)_{ij}(q) \to 0$ when $q \gtrsim \kappa$.

One can define an effective average action corresponding to $S[\varphi]+\Delta S_\kappa[\varphi]$ by $\Gamma_\kappa[\phi]$, where $\phi$ is the average field in the presence of external sources, $\phi_i(x)=\langle\varphi_i(x)\rangle$. When $\kappa=\Lambda$, with $\Lambda$ a scale much larger than all other scales in the problem, fluctuations are suppressed and $\Gamma_\Lambda[\phi]$ coincides with the classical action. As $\kappa$ decreases, more and more fluctuations are taken into account and, as $\kappa \to 0$, $\Gamma_{\kappa=0}[\phi]$ becomes the usual effective action $\Gamma[\phi]$ (see, e.g., Ref. 16). The variation with $\kappa$ of $\Gamma_\kappa[\phi]$ is governed by the following flow equation:[12–14,37]

$$\partial_\kappa \Gamma_\kappa[\phi] = \frac{1}{2}\int \frac{d^dq}{(2\pi)^d}\mathrm{tr}\{\partial_\kappa R_\kappa(q^2)[\Gamma_\kappa^{(2)} + R_\kappa]^{-1}_{q;-q}\}, \tag{2}$$

where $\Gamma_\kappa^{(2)}$ denotes the matrix of second derivatives of $\Gamma_\kappa$ with respect to $\phi$ [i.e., the matrix of components $(\Gamma_\kappa^{(2)})_{ij} = \delta^2\Gamma_\kappa/\delta\phi_i\delta\phi_j$] and the trace is taken over internal indices.

For a given value of $\kappa$, we define the $n$-point vertices $\Gamma_\kappa^{(n)}$ in a constant external field $\phi$:

$$\begin{aligned}(2\pi)^d\delta^{(d)}\left(\sum_j p_j\right)(\Gamma_\kappa^{(n)})_{i_1,i_2,\ldots,i_n}(p_1,\ldots,p_n;\phi) \\ = \int d^dx_1 \cdots \int d^dx_n \exp\left(i\sum_{j=1}^n p_j x_j\right) \\ \times \left|\frac{\delta^n\Gamma_\kappa}{\delta\phi_{i_1}(x_1)\cdots\delta\phi_{i_n}(x_n)}\right|_{\phi(x)\equiv\phi}.\end{aligned} \tag{3}$$

By differentiating Eq. (2) with respect to $\phi_{i_1}(x_1),\ldots,\phi_{i_n}(x_n)$ and then letting the field be constant, one gets the flow equations for all $n$-point functions in a constant background field $\phi$. These equations can be represented diagrammatically by one-loop diagrams with dressed vertices and propagators (see, e.g., Ref. 16). For instance, the flow of the two-point function in a constant external field reads

$$\begin{aligned}\partial_t\Gamma^{(2)}_{ab}(p;\phi) = \int \frac{d^dq}{(2\pi)^d}\partial_t(R_\kappa)_{in}(q)\Big\{ & G_{ij}(q;\phi)\Gamma^{(3)}_{ajk}(p,q,-p \\ & -q;\phi)G_{kl}(q+p;\phi)\Gamma^{(3)}_{blm}(-p,p+q, \\ & -q;\phi)G_{mn}(q;\phi) - \frac{1}{2}G_{ij}(q;\phi)\Gamma^{(4)}_{abjk}(p,-p,q, \\ & -q;\phi)G_{kn}(q;\phi)\Big\},\end{aligned} \tag{4}$$

where $G$ is the matrix of propagators:

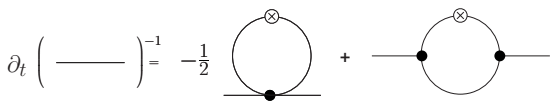

FIG. 1. A diagrammatic representation of the flow equation for the two-point function in an external field. The lines and dots represent full propagators and vertices. Crosses represent the insertion of $\partial_t R_\kappa$.

$$G_\kappa^{-1}(q^2;\phi) = \Gamma_\kappa^{(2)}(q,-q;\phi) + R_\kappa(q^2). \tag{5}$$

The diagrammatic representation of Eq. (4) is given in Fig. 1. Above, we have introduced the dimensionless variable $t \equiv \ln(\kappa/\Lambda)$. From now on, as we already did in Eq. (4), the $\kappa$ dependence of the $n$-point functions shall not be made explicit, unless necessary to avoid confusions.

Flow equations for the $n$-point functions do not close: for example, in order to solve Eq. (4), one needs the three- and the four-point functions, $\Gamma_\kappa^{(3)}$ and $\Gamma_\kappa^{(4)}$, respectively. However, in Ref. 34, an approximation scheme was introduced in order to solve flow equations yielding $n$-point functions at finite momenta. In doing so, it is possible to exploit two properties of these flow equations: (i) Due to the factor $\partial_t R_\kappa(q)$ in the loop integral, the integration is dominated by momenta $q \lesssim \kappa$. (ii) As they are regulated in the IR, $n$-point vertices are smooth functions of momenta. These two properties allow one to make an expansion in powers of $q^2/\kappa^2$, independently of the value of the external momenta $p$. As a typical $n$-point function entering the flow has the form $\Gamma_\kappa^{(n)}(p_1,p_2,\ldots,p_{n-1}+q,p_n-q;\phi)$, where $q$ is the loop momentum, then the *leading order* (LO) of the approximation scheme consists in neglecting the $q$ dependence of such vertex functions:

$$\Gamma^{(n)}(p_1,p_2,\ldots,p_{n-1}+q,p_n-q;\phi) \sim \Gamma^{(n)} \times (p_1,p_2,\ldots,p_{n-1},p_n;\phi). \tag{6}$$

Note that this approximation is *a priori* well justified. Indeed, when all the external momenta $p_i$ are zero, this kind of approximation is at the basis of DE which, as discussed above, turns out to be a good approximation. When the external momenta $p_i$ start to grow, the approximation in Eq. (6) becomes better and better, and it is trivial when all momenta are much larger than $\kappa$. With this approximation, Eq. (4), for instance, becomes

$$\partial_t \Gamma_{ab}^{(2)}(p;\phi) = \int \frac{d^d q}{(2\pi)^d} \partial_t (R_\kappa)_{in}(q) \Big\{ G_{ij}(q;\phi)\Gamma_{ajk}^{(3)}(p,0,-p;\phi) G_{kl}(q+p;\phi)\Gamma_{blm}^{(3)}(-p,p,0;\phi) G_{mn}(q;\phi) - \frac{1}{2} G_{ij}(q;\phi)\Gamma_{abjk}^{(4)}(p,-p,0,0;\phi) G_{kn}(q;\phi) \Big\}. \tag{7}$$

Notice that it is not convenient to also assume $q=0$ in the propagators; if this were done, the exactness of the LO of the approximation scheme both at one-loop or large $N$ limit would be lost (see Ref. 34).

Now, one can exploit the fact that

$$\Gamma_{i_1,i_2,\ldots,i_n,i_{n+1}}^{(n+1)}(p_1,p_2,\ldots,p_n,0;\phi) = \frac{\partial \Gamma_{i_1,i_2,\ldots,i_n}^{(n)}(p_1,p_2,\ldots p_n;\phi)}{\partial \phi_{i_n+1}} \tag{8}$$

in order to transform Eq. (7) into a *closed equation* [recall that $G_\kappa$ and $\Gamma_\kappa^{(2)}$ are related by Eq. (5)]:

$$\partial_t \Gamma_{ab}^{(2)}(p;\phi) = \int \frac{d^d q}{(2\pi)^d} \partial_t (R_\kappa)_{in}(q) \times \Big\{ G_{ij}(q,\phi) \frac{\partial \Gamma_{ak}^{(2)}(p,-p;\phi)}{\partial \phi_j} G_{kl}(q+p,\phi) \frac{\partial \Gamma_{bl}^{(2)}(p,-p;\phi)}{\partial \phi_m} G_{mn}(q,\phi) - \frac{1}{2} G_{ij}(q,\phi) \frac{\partial^2 \Gamma_{ab}^{(2)}(p,-p;\phi)}{\partial \phi_j \partial \phi_k} G_{kn}(q,\phi) \Big\}. \tag{9}$$

Equation (9) is valid for an arbitrary theory with $N$ bosonic fields. In the general case, it corresponds to a system of $N(N+1)/2$ equations. From now on, we shall specialize in the particular case where the bare action $S[\varphi]$ has $O(N)$ symmetry. If one chooses $S[\varphi]$ to be renormalizable, it is given by

$$S[\varphi] = \int d^d x \Big\{ \frac{1}{2}[\partial_\mu \varphi_i(x) \partial_\mu \varphi_i(x)] + \frac{r}{2}\varphi_i(x)\varphi_i(x) + \frac{u}{4!}[\varphi_i(x)\varphi_i(x)]^2 \Big\}. \tag{10}$$

In order to preserve the $O(N)$ symmetry all along the flow, it is mandatory to consider a regulator respecting the symmetry. Doing so, within this approximation scheme, Ward identities shall be respected throughout all the flow and, in particular, they shall de valid in the $(\kappa \to 0)$ physical limit. The only way to implement this is to consider a diagonal regulator. From now on,

$$(R_\kappa)_{ij}(q) = R_\kappa(q)\delta_{ij}.$$

Now, due to the symmetry, the two-point matrix function can be written in terms of only two independent scalar functions; a convenient way to do so is

$$\Gamma_{ab}^{(2)}(p,-p;\phi;\kappa) = \Gamma_A(p;\rho;\kappa)\delta_{ab} + \phi_a\phi_b\Gamma_B(p;\rho;\kappa), \tag{11}$$

where $\rho(x) = \phi^a(x)\phi^a(x)/2$, $a=1,\ldots,N$. Following Eq. (5), a similar decomposition can be done for the propagator matrix. Nevertheless, in this case, it proves more convenient to use a decomposition in longitudinal and transverse components with respect to the external field:

$$G_{ab}(p;\phi;\kappa) = G_T(p;\rho;\kappa)\left(\delta_{ab} - \frac{\phi_a\phi_b}{2\rho}\right) + G_L(p;\rho;\kappa)\frac{\phi_a\phi_b}{2\rho}. \tag{12}$$

It is easy to show that

$$G_T^{-1}(p;\rho;\kappa) = \Gamma_A(p;\rho;\kappa) + R_\kappa(p), \tag{13}$$

$$G_L^{-1}(p;\rho;\kappa) = \Gamma_A(p;\rho;\kappa) + 2\rho\Gamma_B(p;\rho;\kappa) + R_\kappa(p). \tag{14}$$

Using the definition of the functions $\Gamma_A$ and $\Gamma_B$, Eq. (11), as well as that of $G_T$ and $G_L$ given above, the flow equation (9) can be decomposed in two equations for $\Gamma_A$ and $\Gamma_B$:

$$\begin{aligned}\partial_t\Gamma_A(p;\rho) &= 2\rho\Gamma_A'^2(p,\rho)J^{(3)}_{d;LT}(p,\rho) + 2\rho\Gamma_B^2(p;\rho)J^{(3)}_{d;TL}(p;\rho) \\ &\quad - \frac{1}{2}\{[\Gamma_A'(p;\rho) + 2\rho\Gamma_A''(p;\rho)]I^{(2)}_{d;LL}(\rho) + [(N \\ &\quad - 1)\Gamma_A'(p;\rho) + 2\Gamma_B(p;\rho)]I^{(2)}_{d;TT}(\rho)\},\end{aligned} \tag{15}$$

$$\begin{aligned}\partial_t\Gamma_B(p,\rho) &= [\Gamma_A'(p;\rho) + 2\Gamma_B(p;\rho) + 2\rho\Gamma_B'(p;\rho)]^2 J^{(3)}_{d;LL}(p;\rho) \\ &\quad + (N-1)\Gamma_B^2(p;\rho)J^{(3)}_{d;TT}(p;\rho) - \Gamma_A'^2(p;\rho)J^{(3)}_{d;LT}(p;\rho) \\ &\quad - \Gamma_B^2(p;\rho)J^{(3)}_{d;TL}(p;\rho) - \frac{1}{2}\{(N-1)\Gamma_B'(p;\rho)I^{(2)}_{d;TT}(\rho) \\ &\quad + [5\Gamma_B'(p;\rho) + 2\rho\Gamma_B''(p;\rho)]I^{(2)}_{d;LL}(\rho)\} \\ &\quad + \Gamma_B(p;\rho)\int \frac{d^dq}{(2\pi)^d}\{\partial_t R_\kappa(q)\Gamma_B(q;\rho)[G_L(q;\rho) \\ &\quad + G_T(q;\rho)]G_L(q;\rho)G_T(q;\rho)\}.\end{aligned} \tag{16}$$

Above, and from now on, the prime denotes derivative with respect to $\rho$ and, extending definitions already given in Ref. 36, we have introduced the functions

$$I^{(n)}_{d;\alpha\beta}(\rho;\kappa) = \int \frac{d^dq}{(2\pi)^d}\partial_t R_\kappa(q)G_\alpha^{n-1}(q;\rho)G_\beta(q;\rho), \tag{17}$$

$$J^{(n)}_{d;\alpha\beta}(p;\rho;\kappa) = \int \frac{d^dq}{(2\pi)^d}\partial_t R_\kappa(q)G_\alpha^{n-1}(q;\rho)G_\beta(p+q;\rho), \tag{18}$$

with $\alpha$ and $\beta$ standing for either $L$ or $T$. In Eq. (16), we made use of the identity

$$\begin{aligned}[G_T^2(q;\rho) - G_L^2(q;\rho)]\frac{1}{\rho} &= 2\Gamma_B(q;\rho)[G_L(q;\rho) \\ &\quad + G_T(q;\rho)]G_L(q;\rho)G_T(q;\rho)\end{aligned}$$

in order to render the expressions manifestly regular at $\rho = 0$.

Equations (15) and (16) constitute a set of coupled integrodifferential equations, with respect to the real variables $\kappa$, $\rho$, and the modulus of the momentum $p$.

Before turning to the strategy to solve it, we shall first comment on an apparent inconsistency of this approximation procedure and the way to avoid it.[36] To do so, notice that the $n$-point functions at zero external momenta can all be considered as derivatives of a single function, the effective potential $V_\kappa(\rho)$. That is, for example,

$$\Gamma^{(2)}_{ab}(p=0;\rho) = \frac{\partial^2 V_\kappa(\rho)}{\partial\phi_a\partial\phi_b}, \tag{19}$$

which entails

$$\Gamma_A(p=0;\rho) = \frac{\partial V_\kappa(\rho)}{\partial\rho}, \quad \Gamma_B(p=0;\rho) = \frac{\partial^2 V_\kappa(\rho)}{\partial\rho^2}. \tag{20}$$

Now, the effective potential satisfies an exact flow equation which can be deduced from that for the effective action, Eq. (2), when restricted to constant fields. It reads

$$\begin{aligned}\partial_t V_\kappa(\rho) &= \frac{1}{2}\int \frac{d^dq}{(2\pi)^d}\partial_t R_\kappa(q)\{(N-1)G_T(q;\rho) + G_L(q;\rho)\} \\ &= \frac{1}{2}\{(N-1)I^{(1)}_{d;T}(\rho;\kappa) + I^{(1)}_{d;L}(\rho;\kappa)\}.\end{aligned} \tag{21}$$

[In the last term of the equation, we made a slight abuse of language with respect to the definition of Eq. (17): The function $I^{(1)}_{d;\alpha}$ has a unique index $\alpha$ because it contains a unique propagator.]

According to Eq. (19), the second derivative of Eq. (21) with respect to the background field gives a flow equation for $\Gamma^{(2)}_{ab}(p=0;\rho)$. Now, this equation does not coincide with Eq. (9) with $p=0$. Indeed, in contrast to Eq. (9), the vertices in the equation deduced from Eq. (21) keep all their $q$ dependence ($q$ being the momentum in the loop integral); in other words, it is a more precise equation. There is therefore an apparent inconsistency between Eqs. (9), (19), and (21). However, this can be easily solved. To do so, it is convenient to treat separately the zero momentum ($p=0$) and the nonzero momentum ($p \neq 0$) sectors (for a further discussion, see Ref. 36).

Let us then define

$$\Delta_A(p;\rho;\kappa) \equiv \Gamma_A(p;\rho;\kappa) - p^2 - \Gamma_A(p=0;\rho;\kappa), \tag{22}$$

$$\Delta_B(p;\rho;\kappa) \equiv \Gamma_B(p;\rho;\kappa) - \Gamma_B(p=0;\rho;\kappa). \tag{23}$$

The flow equations for $\Delta_A$ and $\Delta_B$ easily follow from those for $\Gamma_A$ and $\Gamma_B$:

$$\partial_t\Delta_A(p;\rho) = \partial_t\Gamma_A(p;\rho;\kappa) - \partial_t\Gamma_A(p=0;\rho;\kappa) \tag{24}$$

and equivalently for $\Delta_B(p;\rho;\kappa)$.

The procedure we shall consider in this paper consists then in solving simultaneously the three flow equations for $V_\kappa(\rho)$ [Eq. (21)], $\Delta_A(p;\rho;\kappa)$, and $\Delta_B(p;\rho;\kappa)$ and then get two-point functions through

$$\Gamma_A(p;\rho;\kappa) = p^2 + \Delta_A(p;\rho;\kappa) + \frac{\partial V_\kappa(\rho)}{\partial\rho}, \tag{25}$$

$$\Gamma_B(p;\rho;\kappa) = \Delta_B(p;\rho;\kappa) + \frac{\partial^2 V_\kappa(\rho)}{\partial\rho^2}. \tag{26}$$

The initial conditions for the flow are $V_\Lambda(\rho) = r_\Lambda\rho + (u/6)\rho^2$ [see Eq. (10)] for the potential, while those for both $\Delta$ functions are equal to 0, as the classical momentum dependence is explicitly taken out in their definition [see Eqs. (22) and (23)]. Notice that, proceeding in this way, not only we maintain the validity of the relationship given by Eq. (19), but we also gain more accuracy in the description of the two-point function. Indeed, its momentum independent part is now described with a higher precision, while the approximation in-

troduced in Ref. 34, which is used in this paper, only affects its $p$ dependence.

## III. RESOLUTION STRATEGIES

Although the flow equations for $V_\kappa(\rho)$, $\Delta_A(p;\rho;\kappa)$, and $\Delta_B(p;\rho;\kappa)$ can, in principle, be solved numerically, this nonetheless constitutes a rather cumbersome task. The reason is twofold. First, what we called $I$ and $J$ are, in fact, functionals of the solution $\Gamma^{(2)}(p,\rho;\kappa)$; this complicates the possible integration strategies. Second, notice that different values of $p$ are coupled through the propagators $G_\alpha(p+q;\kappa)$ which enter in the calculations of the $J$ functions; this demands, in principle, the simultaneous solution of the equations for all $p$.

Nevertheless, we shall show that within a simple, and yet accurate, further approximation, our flow equations become numerically simpler. In this section, we shall, in fact, discuss two possible approximation strategies.

### A. First level of approximation: Strategy I

In order to simplify the above mentioned issues, and to bring down the numerical effort necessary to solve our set of NPRG equations, it is possible to perform a further approximation (see Ref. 36, where the same approximation was used in the $N=1$ case and an assessment of its accuracy was done).

Consider first the function $I^{(n)}_{d,\alpha\beta}(\rho;\kappa)$, which does not depend on $p$. The smoothness of the $n$-point functions and the fact that integrals are dominated by the domain $q \lesssim \kappa$ suggest performing in the propagators of the right-hand side of Eq. (17) an approximation similar to that applied to the other $n$-point functions, i.e., to set $q=0$. However, as already said in the previous section, in order to maintain both the exact one-loop and large $N$ properties of the flow equations, one cannot simply set $q=0$ in the whole propagator; rather, one needs a momentum dependence recovering that of the free propagators in the $\kappa \to \Lambda$ limit. Thus, we shall use for the propagators entering the calculation of $I^{(n)}_{d;\alpha\beta}(\rho;\kappa)$ the following approximate forms:

$$G_T^{-1}(q;\rho;\kappa) \approx Z_\kappa q^2 + \Gamma_A(q=0;\rho;\kappa) + R_\kappa(q), \tag{27}$$

$$G_L^{-1}(q;\rho;\kappa) \approx Z_\kappa q^2 + \Gamma_A(q=0;\rho;\kappa) + 2\rho\Gamma_B(q=0;\rho;\kappa) + R_\kappa(q), \tag{28}$$

where

$$Z_\kappa \equiv \left.\frac{\partial \Gamma^{(2)}_\kappa}{\partial q^2}\right|_{q=0,\rho=\rho_0}. \tag{29}$$

As we shall see in the following, the presence of the $Z_\kappa$ factor is needed in order to preserve scaling properties. As it is well known,[14] $\partial\Gamma^{(2)}(q;\rho)/\partial q^2|_{q=0}$ depends weakly on $\rho$. Accordingly, one expects $Z_\kappa$ to depend weakly on the value chosen for $\rho_0$. As argued in Ref. 36, the choice $\rho_0=0$ is here the simplest one. With the propagators of Eqs. (27) and (28), and the choice of the regulating function[19]

$$R_\kappa(q) = Z_\kappa(\kappa^2 - q^2)\Theta(\kappa^2 - q^2), \tag{30}$$

the function $I^{(n)}_{d;\alpha\beta}(\rho;\kappa)$ can be calculated analytically:

$$I^{(n)}_{d,\alpha\beta}(\rho;\kappa) = 2K_d \frac{\kappa^{d+2-2n}}{Z_\kappa^{n-1}}\left(1 - \frac{\eta_\kappa}{d+2}\right) \times \frac{1}{[1+\hat{m}^2_\alpha(\rho)]^{n-1}[1+\hat{m}^2_\beta(\rho)]}. \tag{31}$$

In this expression,

$$\eta_\kappa \equiv -\kappa\partial_\kappa \ln Z_\kappa \tag{32}$$

is the running anomalous dimension and

$$\hat{m}^2_T(\rho;\kappa) \equiv \frac{\Gamma_A(q=0;\rho;\kappa)}{\kappa^2 Z_\kappa} = \frac{V'_\kappa(\rho)}{\kappa^2 Z_\kappa}, \tag{33}$$

$$\hat{m}^2_L(\rho;\kappa) \equiv \frac{\Gamma_A(q=0;\rho;\kappa) + 2\rho\Gamma_B(q=0;\rho;\kappa)}{\kappa^2 Z_\kappa} = \frac{V'_\kappa(\rho) + 2\rho V''_\kappa(\rho)}{\kappa^2 Z_\kappa} \tag{34}$$

are dimensionless, field-dependent effective masses. Above, $K_d$ is a number resulting from angular integration, $K_d^{-1} \equiv d2^{d-1}\pi^{d/2}\Gamma(d/2)$ [e.g., $K_3 = 1/(6\pi^2)$]. Notice that, for $d>2$, $I^{(2)}_{d,\alpha\beta}(\kappa;\rho) \to 0$ when $\kappa \to 0$.

As for the function $J^{(n)}_{d,\alpha\beta}(p;\rho;\kappa)$, we shall calculate it in a similar way. To do so, let us notice that the propagator $G_\alpha(p+q;\rho)$ in Eq. (18) is small as soon as $p/\kappa$ is large; one can verify that the function $J^{(3)}_{d,\alpha\beta}(p;\rho;\kappa)$ vanishes approximately as $\kappa^2/p^2$ for large values of $p/\kappa$. Thus, in the region where $J^{(3)}_{d,\alpha\beta}(p;\rho;\kappa)$ has a non-negligible value, one can assume $p \lesssim \kappa$ and then use for $G_\alpha(p+q;\rho)$ an expression similar to that of Eq. (27) or (28), namely,

$$G_T^{-1}(p+q;\rho;\kappa) \approx Z_\kappa(p+q)^2 + \Gamma_A(q=0;\rho;\kappa) + R_\kappa(p+q), \tag{35}$$

$$G_L^{-1}(p+q;\rho;\kappa) \approx Z_\kappa(p+q)^2 + \Gamma_A(0;\rho;\kappa) + 2\rho\Gamma_B(q=0;\rho;\kappa) + R_\kappa(p+q). \tag{36}$$

One can then calculate the functions $J^{(3)}_{d,\alpha\beta}(p;\rho;\kappa)$ analytically [in $d=3$ and with the regulator of Eq. (30)]. The resulting expressions are more complicated than those for $I^{(2)}_{d,\alpha\beta} \times(\rho;\kappa)$, Eq. (31). They are given in Appendix B. Observe that the regulator in Eq. (30) is not analytic at $q=\kappa$. This generates nonanalyticities in $J^{(3)}_{d,\alpha\beta}(p;\rho;\kappa)$, but these occur only in the third derivative with respect to $p$, at $p=0$, and at $p=2\kappa$ [cf., e.g., the odd powers of $\bar{p}$ in Eqs. (B1)–(B4)], and they play no role at the present level of approximation.

Finally, for the last term in Eq. (16), it is possible to use the same approximation procedure described above; doing so, $\Gamma_B(q;\rho) \simeq \Gamma_B(q=0;\rho) = V''(\rho)$, and the term is then just proportional to the sum of two $I^{(3)}$ functions.

With the approximation just discussed, both $I^{(n)}_{d,\alpha\beta}(\rho;\kappa)$ and $J^{(3)}_{d,\alpha\beta}(p;\rho;\kappa)$ become explicit functions of the potential $V_\kappa(\rho)$ and the field renormalization constant $Z_\kappa$ [or, equiva-

lently, $\eta_\kappa$, see Eq. (32)]. From now on, we shall denote the range of momenta $p \lesssim \kappa$, which is described by quantities as $V_\kappa(\rho)$ and $Z_\kappa$ (or $\eta_\kappa$) as the "$p=0$ sector" of the theory.

To finish the description of the calculation procedure, it is then necessary to make explicit how to solve these two flow equations. The simplest way is the usual procedure of DE. Specific details are presented in Appendix A. Here, we shall just quote three ingredients which are relevant for our present discussion. First notice that, within DE, the integral $I^{(1)}_{d;\alpha}$ appearing in the potential flow equation is calculated using the approximate propagators from Eqs. (27) and (28), i.e., the integral is given by Eq. (31). We shall be back to this point in the next section. Second, in order to get the proper scaling behavior of $\Gamma^{(2)}(p;\rho;\kappa)$ at small momenta, we need the flow equation for $Z_\kappa$ to be consistent with the approximate Eq. (9) for the two-point function. This is achieved by extracting $Z_\kappa$ from the flow equation of $\lim_{p\to 0}\Delta_A(p;\rho=0;\kappa)/p^2$, which follows from Eq. (9), and invoking Eq. (29). Details can be found in Appendix A. Third, let us notice that, in fact, the flow equation for the potential is qualitatively different than those for $\Delta_A(p;\rho;\kappa)$ and $\Delta_B(p;\rho;\kappa)$. Indeed, these depend on a dimensionful quantity $p$; thus, when $\kappa \to 0$, the corresponding flow stops, giving a finite value for both two-point functions, which depends on $p$. On the other side, at criticality, the potential only depends on the dimensionful physical variable $\rho$, whose relevant values shrink to zero when $\kappa \ll u$; the system is then characterized by scale invariance. In order to correctly parametrize this property, it is convenient to work with dimensionless variables

$$\tilde{\rho} \equiv K_d^{-1} Z_\kappa \kappa^{2-d} \rho, \quad v_\kappa(\tilde{\rho}) \equiv K_d^{-1} \frac{V_\kappa(\rho)}{\kappa^d}. \tag{37}$$

Doing so, the dimensionless potential $v_\kappa(\tilde{\rho})$ approaches a nontrivial fixed point form when $\kappa \ll u$.

The strategy to solve Eq. (9) for the flow of the two-point function consists then in two steps One first solves the $p=0$ sector to get $v_\kappa(\tilde{\rho})$ and $\eta_\kappa$; in doing so, the bare mass is adjusted in order to reach the IR fixed point. Second, for each value of $p$, one solves the flow equations for the $\Delta$'s, where the kernels $I^{(n)}_d(\rho;\kappa)$ and $J^{(3)}_d(p;\rho;\kappa)$ are explicit functions of $v_\kappa(\rho)$, $Z_\kappa$, and $\eta_\kappa$. The problem of finding the two-point function of the $O(N)$ symmetric scalar field is thus reduced to the solution of a system of partial differential equations with parameter $p$, which can be solved separately for each value of $p$ and which does not involve a numerical effort greater than that required in usual DE calculations.

### B. Improved approximation: Strategy II

In Sec. I, we recalled an interesting property of the approximation scheme introduced in Ref. 34: When solving the flow equation of the two-point function at the LO of the scheme, the effective potential one gets is exact at two loops. Nevertheless, when solving Eq. (21) using the propagators described in the previous section, this two-loop exactness is lost. We shall present now a simple improvement in the procedure proposed in Sec. III A in order to recover the two-loop expression for the potential. This should bring a better description of the $p=0$ sector of the model, which would be particularly useful for the determination of critical exponents.

In order to do so, let us briefly note the origin of the two-loop exactness. It exploits the fact that only one-loop two diagrams contribute to the flow [see, for example, Eqs. (2), (4), and (21), or Fig. 1]. Accordingly, the two-point function gets exact at one loop, provided its flow is calculated with quantities which are exact in the classical limit. This is respected not only within the approximate Eq. (9) but also after the extra approximation in the propagators introduced in Sec. III A. As for the potential, Eq. (21) gives indeed an exact expression at two loops only if the flow is calculated with quantities exact at one loop. This is, in principle, the case for the equations here considered. Nevertheless, the extra approximation introduced in Sec. III A, when applied to the potential flow equation, violates this property. Fortunately, this can be swiftly solved and with a low numerical cost.

This improvement can be achieved by numerically integrating the function $I^{(1)}$ appearing in the flow equation for the potential, without using the approximate propagator of Eqs. (27) and (28), but, instead, the numerical solutions for $\Delta_A$ and $\Delta_B$:

$$\partial_t V_\kappa(\rho) = \frac{1}{2}\int \frac{d^d q}{(2\pi)^d} \partial_t R_\kappa(q) \Bigg( (N-1) \times \frac{1}{q^2 + \Delta_A(q;\rho) + V'(\rho) + R_\kappa(q)} + \frac{1}{q^2 + \Delta_A(q;\rho) + 2\rho\Delta_B(q;\rho) + V' + 2\rho V'' + R_\kappa(q)} \Bigg). \tag{38}$$

One thus needs to simultaneously solve the flow equations for $V_\kappa$, $\Delta_A$, and $\Delta_B$.

Notice that the approximate propagators, and thus the analytic expressions for $J$, from Appendix B, and for $I^{(2)}$ and $I^{(3)}$, from Eq. (31), can still be used in the flow equations for $\Delta_A$ and $\Delta_B$ without losing their one-loop exactness.

In Eq. (38), angular integration can be done analytically reducing the problem to a numerical integration over one single variable, $|q|$. Accordingly, the procedure does not introduce too much extra complexity in the algorithm. However, an important subtlety arises: due to the regulator, the integrand of $I^{(1)}$ takes non-negligible values only in the range $|q| \lesssim \kappa$. Thus, with a fixed grid in $q$, as $\kappa$ goes to the physical value $\kappa=0$, the number of points in $q$ for performing a numerical integration in Eq. (38) would dwindle very rapidly.

This apparent difficulty is cured by working with fixed values of $q/\kappa$, i.e., solving the $\Delta$ function flow equations within a grid for fixed values of $\tilde{q} \equiv q/\kappa$ with $\tilde{q} < \tilde{q}_{max}$; values of $\tilde{q}_{max} \sim 3-4$ turn out to be large enough. Nevertheless, due to their definition [see Eqs. (22) and (23)], when $\kappa \to 0$, all functions in the grid would vanish. As usually done for the potential [see Eq. (37)], this difficulty is simply solved working with dimensionless variables:

$$\tilde{\Delta}_A(\tilde{p};\tilde{\rho}) \equiv \frac{\Delta_A(p;\rho)+p^2}{\kappa^2 Z_\kappa}, \quad \tilde{\Delta}_B(\tilde{p};\tilde{\rho}) \equiv \frac{\Delta_B(p;\rho)}{\kappa^{4-d} Z_\kappa^2 K_d^{-1}}. \tag{39}$$

At criticality, these quantities reach finite values in the $\kappa \to 0$ limit, with this limit depending on the value of $\tilde{p}=p/\kappa$. These functions $\tilde{\Delta}_A$ and $\tilde{\Delta}_B$ are precisely the quantities entering the integrand of the flow equation for the dimensionless potential $v_\kappa$ [which follows from Eqs. (37) and (38)].

As a final remark concerning the $p=0$ sector, note that we now have many fixed point flow equations: those for the dimensionless potential $v_\kappa$ and for $\eta_\kappa$ and those for the dimensionless $\tilde{\Delta}$ functions (in fact, two equations for each value of $\tilde{q}$ on the grid). As we are dealing with a Wilson-Fisher fixed point, the flow has only one unstable direction; thus, once only one bare parameter is fined tuned (here, the bare mass), the complete set of equations should reach the fixed point. However, handling the flow equations for $\tilde{\Delta}_A$ and $\tilde{\Delta}_B$ turns out to be a hard numerical task. For reasons of numerical stability, it proves useful to introduce the auxiliary variables

$$Y_A(\tilde{p};\tilde{\rho}) \equiv \frac{\tilde{\Delta}_A(\tilde{p};\tilde{\rho})}{\tilde{p}^2}, \quad Y_B(\tilde{p};\tilde{\rho}) \equiv \frac{\tilde{\Delta}_B(\tilde{p};\tilde{\rho})}{\tilde{p}^2}. \tag{40}$$

Flow equations for $Y_A$ and $Y_B$ are trivially derived. The departing point is the flow equations for $\Delta_A$ and $\Delta_B$ we used in the previous section, i.e., those with the approximated analytic expressions for the functions $J^{(3)}$, $I^{(2)}$, and $I^{(3)}$. Then, making use of Eqs. (39) and (40), a straightforward calculation yields

$$\begin{aligned}
\partial_t Y_A(\tilde{p};\tilde{\rho}) &= \eta Y_A(\tilde{p};\tilde{\rho}) + \tilde{p}\frac{\partial Y_A}{\partial \tilde{p}}(\tilde{p};\tilde{\rho}) + (d-2+\eta)\tilde{\rho}Y_A' + 2\left(1-\frac{\eta}{d+2}\right)\left[-\frac{1}{\tilde{p}^2}\frac{2\tilde{\rho}}{(1+w+2\tilde{\rho}w')^2}\frac{w'^2}{1+w} - \frac{1}{\tilde{p}^2}\frac{2\tilde{\rho}}{(1+w)^2}\frac{w'^2}{1+w+2\tilde{\rho}w'}\right. \\
&\left. - \frac{1}{2}\frac{[Y_A'(\tilde{p};\tilde{\rho})+2\tilde{\rho}Y_A''(\tilde{p};\tilde{\rho})]}{(1+w+2\tilde{\rho}w')^2} - \frac{1}{2}\frac{[(N-1)Y_A'(\tilde{p};\tilde{\rho})+2Y_B(\tilde{p};\tilde{\rho})]}{(1+w)^2}\right] + 2\tilde{\rho}\tilde{J}_{LT}(\tilde{p};\tilde{\rho})\left(Y_A'^2(\tilde{p};\tilde{\rho})\tilde{p}^2 + 2Y_A'(\tilde{p};\tilde{\rho})w' + \frac{w'^2}{\tilde{p}^2}\right) \\
&+ 2\tilde{\rho}\tilde{J}_{TL}(\tilde{p};\tilde{\rho})\left(Y_B^2(\tilde{p};\tilde{\rho})\tilde{p}^2 + 2Y_B(\tilde{p};\tilde{\rho})w' + \frac{w'^2}{\tilde{p}^2}\right),
\end{aligned} \tag{41}$$

$$\begin{aligned}
\partial_t Y_B(\tilde{p};\tilde{\rho}) &= (d-2+2\eta)Y_B(\tilde{p};\tilde{\rho}) + \tilde{p}\frac{\partial Y_B}{\partial \tilde{p}}(\tilde{p};\tilde{\rho}) + (d-2+\eta)\tilde{\rho}Y_B'(\tilde{p};\tilde{\rho}) + 2\left(1-\frac{\eta}{d+2}\right)\left[\frac{(N-1)w'^2}{\tilde{p}^2(1+w)^3}\right. \\
&+ \frac{(9w^2+12\tilde{\rho}w'w''+4\tilde{\rho}^2w''^2)}{\tilde{p}^2(1+w+2\tilde{\rho}w')^3} - \frac{1}{\tilde{p}^2}\frac{1}{(1+w+2\tilde{\rho}w')^2}\frac{w'^2}{1+w} - \frac{1}{\tilde{p}^2}\frac{1}{(1+w+2\tilde{\rho}w')}\frac{w'^2}{(1+w)^2} - \frac{1}{2}\frac{(N-1)}{(1+w)^2}Y_B'(\tilde{p};\tilde{\rho}) \\
&\left. - \frac{1}{2}\frac{[5Y_B'(\tilde{p};\tilde{\rho})+2\tilde{\rho}Y_B''(\tilde{p};\tilde{\rho})]}{(1+w+2\tilde{\rho}w')^2} + \left(\frac{1}{1+w+2\tilde{\rho}w'}+\frac{1}{1+w}\right)\frac{1}{1+w}\frac{Y_B(\tilde{p};\tilde{\rho})w'}{1+w+2\tilde{\rho}w'}\right] + (N-1)\tilde{J}_T(\tilde{p};\tilde{\rho})\left(Y_B^2(\tilde{p};\tilde{\rho})\tilde{p}^2\right. \\
&\left. + Y_B(\tilde{p};\tilde{\rho})w' + \frac{w'^2}{\tilde{p}^2}\right) + \tilde{J}_L(\tilde{p};\tilde{\rho})\left\{Y_A'^2(\tilde{p};\tilde{\rho})\tilde{p}^2 + 4Y_B^2(\tilde{p};\tilde{\rho})\tilde{p}^2 + 6Y_A'(\tilde{p};\tilde{\rho})w' + \frac{9w'^2}{\tilde{p}^2} + 4Y_A'(\tilde{p};\tilde{\rho})Y_B(\tilde{p}\tilde{p}^2;\tilde{\rho})\right. \\
&+ 12Y_B(\tilde{p};\tilde{\rho})w' + 4\tilde{\rho}\left(Y_A'(\tilde{p};\tilde{\rho})Y_B'(\tilde{p};\tilde{\rho})\tilde{p}^2 + Y_A'(\tilde{p};\tilde{\rho})w'' + 3Y_B'(\tilde{p};\tilde{\rho})w' + \frac{3w'w''}{\tilde{p}^2} + 2Y_B(\tilde{p};\tilde{\rho})Y_B'(\tilde{p};\tilde{\rho})\tilde{p}^2\right. \\
&\left.\left. + 2Y_B(\tilde{p};\tilde{\rho})w'' + 2Y_B'(\tilde{p};\tilde{\rho})w' + 4\tilde{\rho}^2[Y_B'^2(\tilde{p};\tilde{\rho})] + 2Y_B'(\tilde{p};\tilde{\rho})w'' + \frac{w''^2}{\tilde{p}^2}\right)\right\} - \tilde{J}_{LT}(\tilde{p};\tilde{\rho})\left(Y_A'^2(\tilde{p};\tilde{\rho})\tilde{p}^2 + 2Y_A'(\tilde{p};\tilde{\rho})w'\right. \\
&\left. + \frac{w'^2}{\tilde{p}^2}\right) - \tilde{J}_{TL}(\tilde{p};\tilde{\rho})\left(Y_B^2(\tilde{p};\tilde{\rho})\tilde{p}^2 + 2Y_B(\tilde{p};\tilde{\rho})w' + \frac{w'^2}{\tilde{p}^2}\right).
\end{aligned} \tag{42}$$

Notice that the process of going to dimensionless variables brought into play derivatives with respect to $\tilde{p}$. Above, we introduced the dimensionless expression $\tilde{J}_{\alpha\beta}(\tilde{p};\tilde{\rho})$ of the function $J$, which is given in Appendix B. The $(\kappa=\Lambda)$ initial values for these functions are $Y_A=1$ and $Y_B=0$.

In summary, according to this second strategy to get the two-point functions of the $O(N)$ model, one also proceeds in two steps. First, one fixes the $p=0$ sector, which now demands the simultaneous solution of the full flow equation for the potential [Eq. (38)] together with those for $Y_A$ and $Y_B$ [Eqs. (41) and (42)] for a limited number of values of $\tilde{q} < \tilde{q}_{max}$. Proceeding this way, one fine tunes the bare mass in order to get the infrared fixed point. As a second step, one solves the flow equations for dimensionful $\Delta_A$ and $\Delta_B$ (the same one as those of the previous section) for any desired

value of the external momenta $p$. Within this second strategy, once the $p=0$ sector is solved, the $p\neq 0$ sector can still be treated separately for each value of $p$.

Using the alternative idea just presented, one hopes to have a better description of the $p=0$ sector and, thus, to get an improvement in critical exponents and infrared properties of the model. Moreover, one can also hope to retrieve better results at least in the crossover region between IR and UV behaviors.

## IV. NUMERICAL RESULTS AND DISCUSSION

We now turn to the numerical solutions obtained within both of the methods we have discussed in the previous section. We shall consider here the properties of the system near or at criticality, and we shall study the $d=3$ case. Our goal here is twofold: First is to assess the quality of the approximation scheme at all ranges of momenta and to verify what is the effect of the improvement discussed in the last subsection. Second, since we are working here only with the LO of the approximation method proposed in Ref. 34 (and, moreover, using approximate propagators), we aim to compare our results with those already existing in the literature for the $O(N)$ model.

It is possible to distinguish three momentum regions: the IR sector ($p \ll u$), the UV sector ($p \gg u$), and the intermediate crossover sector. The first region is dominated by scaling properties and has been studied using many different methods with high precision. In the next section, we shall present our predictions for this regime, paying particular attention to scaling properties and comparing our results with those existent in the literature. As for the UV regime, it can also be described with high precision within perturbative calculations. Finally, the crossover region is known with much less accuracy; it is therefore the main yield of this work. Both the UV and the crossover regimes shall be discussed in the second part of this section.

### A. Scaling properties

When $\kappa \ll p \ll u$, we expect $\Delta_A(p;\kappa)$ to behave as

$$p^2 + \Delta_A(p;\kappa) = A p^{2-\eta^*}, \tag{43}$$

where $\eta^*$ is the anomalous dimension, i.e., the fixed point value of $\eta_\kappa$. As the explicit $p$ dependence of the two-point function is very hard to obtain, in the literature, the usual way to determine $\eta^*$ is to extract it from the $\kappa$ dependence of $Z_\kappa$ [see Eq. (32)]:

$$Z_\kappa \propto \kappa^{-\eta^*}, \tag{44}$$

when $\kappa \ll u$. Nevertheless, although these two extractions should, in principle, lead to the same result,[29] when approximating, the flow equations this property can be lost. This is, for example, the case in DE which, at criticality, describes physical quantities only at $p=0$; not even the $\kappa \ll p \ll u$ regime is correctly described. We have checked that, for all the solutions we get, we always have the same result within the two extraction methods.

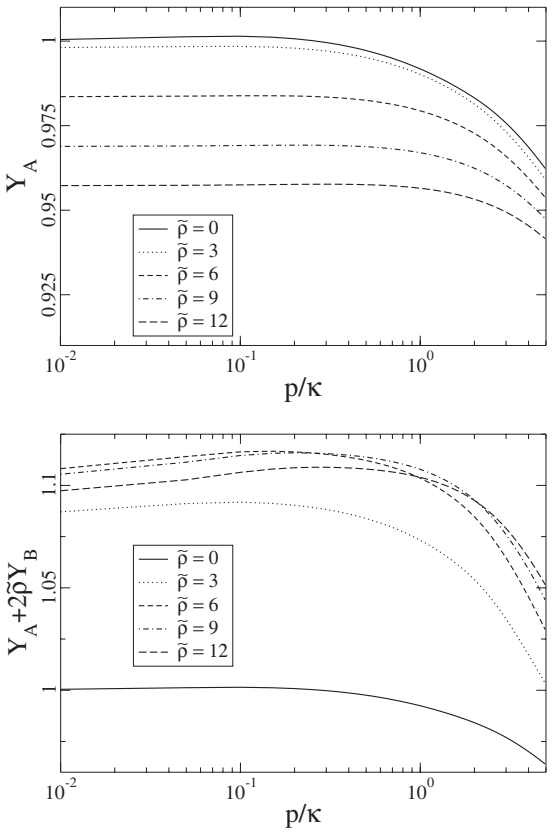


FIG. 2. The fixed point form for the functions $Y_A(\tilde{p},\tilde{\rho})$ and $Y_A(\tilde{p},\tilde{\rho})+2\tilde{\rho}Y_B(\tilde{p},\tilde{\rho})$, in $d=3$, $N=2$, at criticality, as a function of $\tilde{p}$ for various values of $\tilde{\rho}$.

A more stringent test of scaling is given by the study of the dimensionless quantities

$$\frac{\Delta_A(p;\tilde{\rho};\kappa)+p^2}{p^2 Z_\kappa}, \quad \frac{\Delta_A(p;\tilde{\rho};\kappa)+2\rho\Delta_B(p;\tilde{\rho};\kappa)+p^2}{p^2 Z_\kappa}, \tag{45}$$

which, in the scaling regime ($p,\kappa \ll u$), should be functions of only $p/\kappa$ and $\tilde{\rho}$. In fact, according to Eqs. (39) and (40), these should be the scaling functions $Y_A(\tilde{p};\tilde{\rho})$ and $Y_A(\tilde{p};\tilde{\rho})+2\tilde{\rho}Y_B(\tilde{p};\tilde{\rho})$. We have numerically checked that our results verify this property. In Fig. 2, we show these scaling functions, as a function of $\tilde{p}$, for various values of $\tilde{\rho}$ and $N=2$. Similar results are found for other values of $N$.

Notice that, by definition of $Z_\kappa$ [see Eq. (29)], the function $Y_A(\tilde{p}=0,\tilde{\rho}=0)=1$. A nontrivial fact, shown by Fig. 2, is that both the functions $Y_A(\tilde{p},\tilde{\rho})$ and $Y_A(\tilde{p},\tilde{\rho})+2\tilde{\rho}Y_B(\tilde{p},\tilde{\rho})$ are well approximated by unity for all $\tilde{p} \lesssim 1$ and all relevant values of $\tilde{\rho}$ (as well known,[16] the latter are those of the order of the minimum of the potential which, within our normalization, runs from $\tilde{\rho} \sim N+2$, when $\kappa=\Lambda$, to $\tilde{\rho} \sim N$, when $\kappa \to 0$). This is exactly what we assumed within the two numerical approximations introduced in the last section. In other words, the figure shows that, even in the deep IR, the approximated propagators of Eqs. (27) and (28) are indeed accurate. In Ref. 36, where the same approximation is done in order to solve

TABLE I. Critical exponents for the $O(N)$ model. We present our results within the two calculation strategies, together with DE at NLO and the best estimates, with their errors, when available. When results of similar quality can be found in the literature, they are both quoted (for discussion of DE results, see text).

| $N$ | $\eta$ I | $\eta$ II | $\eta$ DE-NLO | $\eta$ (best) | $\nu$ I | $\nu$ II | $\nu$ DE-NLO | $\nu$ (best) |
|---|---|---|---|---|---|---|---|---|
| 0 | 0.0460 | 0.0385 | 0.039[a] | 0.0284(25)[b] | 0.603 | 0.599 | 0.590[a] | 0.5882(11)[b] |
| 1 | 0.0519 | 0.0466 | 0.0467[a] | 0.03639(15)[c] | 0.647 | 0.645 | 0.6307[a] | 0.63012(16)[c] |
| | | | 0.0443[d] | 0.0368(2)[e] | | | 0.6307[d] | 0.63020(12)[e] |
| 2 | 0.0523 | 0.0474 | 0.049[a] | 0.0381(2)[f] | 0.691 | 0.689 | 0.666[a] | 0.6717(1)[f] |
| 3 | 0.0496 | 0.0471 | 0.049[a] | 0.0375(5)[g] | 0.729 | 0.728 | 0.704[a] | 0.7112(5)[g] |
| 4 | 0.0455 | 0.0445 | 0.047[a] | 0.0350(45)[b] | 0.761 | 0.760 | 0.739[a] | 0.741(6)[b] |
| | | | | 0.0365(10)[h] | | | | 0.749(2)[h] |
| 5 | 0.0409 | 0.0407 | | 0.031(3)[i] | 0.786 | 0.786 | | 0.764(4)[i] |
| | | | | 0.034(1)[j] | | | | 0.779(3)[j] |
| 6 | 0.0368 | | | 0.029(3)[i] | 0.816 | | | 0.789(5)[i] |
| 7 | 0.0331 | | | 0.029[k] | 0.838 | | | 0.811[k] |
| 8 | 0.0298 | | | 0.027[k] | 0.856 | | | 0.830[k] |
| 9 | 0.0271 | | | 0.025[k] | 0.864 | | | 0.845[k] |
| 10 | 0.0246 | 0.0253 | 0.028[a] | 0.024[k] | 0.882 | 0.882 | 0.881[a] | 0.859[k] |
| 20 | 0.0127 | | | 0.014[k] | 0.941 | | | 0.930[k] |
| 100 | 0.0025 | 0.00254 | 0.0030[a] | 0.0027[l] | 0.990 | 0.990 | 0.990[a] | 0.989[l] |
| Large $N$ | $0.25/N$ | $0.25/N$ | | $0.270/N$[l] | $1-1.034/N$ | | | $1-1.081/N$[l] |

[a]Reference 39. [d]Reference 38. [g]Reference 5. [j]Reference 8.
[b]Reference 1. [e]Reference 6. [h]Reference 7. [k]Reference 40.
[c]Reference 3. [f]Reference 4. [i]Reference 2. [l]Reference 41.

the $N=1$ case, its effect on the functions $I$ and $J$ is shown to be small. There, only the longitudinal propagator, i.e., that given by Eq. (28), plays a role (remember that the term including the transverse propagator is proportional to $N-1$). Figure 2 shows that the approximation is even better in the transverse case; accordingly, when going to large values of $N$, one expects the approximations introduced in the last section to become better. As we shall see, this is confirmed by our numerical results.

Our estimates for the anomalous dimension for different values of $N$, using both of our methods of approximation, are presented in Table I. We also plot, in Fig. 3, $N\eta$ as a function of $1/N$. When $N$ is not too large, $N \lesssim 4$, strategy II introduces noticeable improvements. For example, for $N=1$, $\eta^*$ changes from $\eta^* \simeq 0.052$ using the first approximation to $\eta^* \simeq 0.047$ using the improved one. These values are to be compared with results obtained by other means. DE gives $\eta^*=0$ at LO[14] and $\eta^*=0.033$ at next-to-NLO.[24] As for the NLO, various results exist. Using the regulator of the present paper, one gets $\eta^*=0.050$ (Ref. 38) and $\eta^*=0.054$ with a power-law regulator[22] and $\eta^*=0.0467$ with an exponential regulator;[39] moreover, after an optimization procedure, results move to $\eta^*=0.0470$, for a thetalike regulator, and $\eta^*=0.0443$, for an exponential one.[38] In the table, we present the best results with and without optimization. Thus, even after the extra approximation introduced in the numerical resolution strategy, the LO of the approximation procedure introduced in Ref. 34 yields a value of the anomalous dimension comparable to that of the DE at NLO. All these NPRG values can be compared with $\eta^*=0.034(3)$ from the resummed seven-loop calculation,[1] $\eta^*=0.0364(2)$ with high-$T$ calculation[3] and $\eta^*=0.0368(2)$ from Monte Carlo (MC).[6]

As $N$ increases, our two calculation strategies differ less and less, and eventually they give the same result. Most remarkably, our yields are very close to those of the DE at NLO, at least for small values of $N$. Note, however, that DE results can depend strongly on the choice of the regulator; with a less reliable regulator, results[22] depart from best estimates. Both this work and DE results reach the correct large $N$ limit: $\eta=0$. The large $N$ regime is better studied with the help of Fig. 3. There, we present the best estimates, as well as DE and the present results, together with the known analytical numbers for both the large $N$ limit and its first order

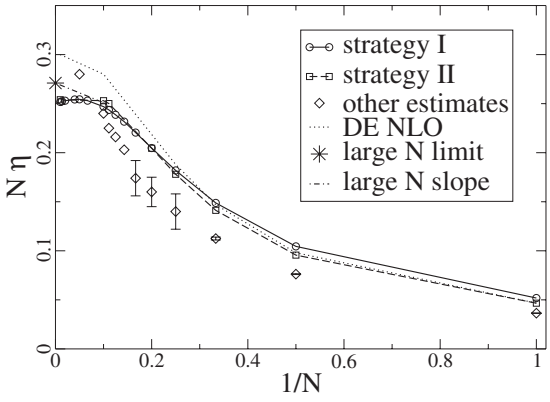


FIG. 3. $N\eta$ as a function of $1/N$ for various model calculations, together with the $1/N$ analytical results.

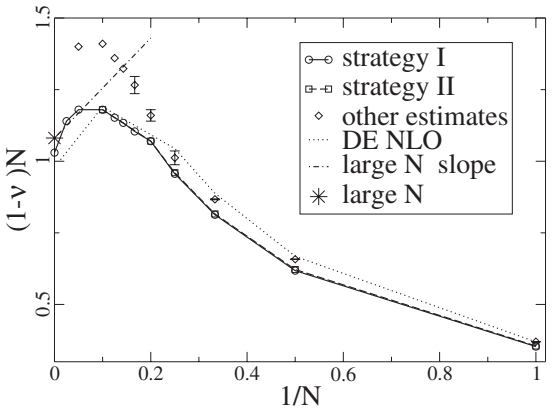


FIG. 4. $N(1-\nu)$ as a function of $1/N$. This quantity is useful to study the large $N$ behavior of the critical exponent $\nu$.

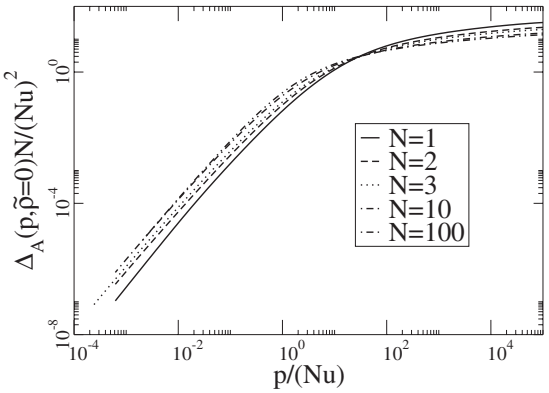


FIG. 5. $\Delta_A(p;\rho=0)N/(u/N)^2$, in $d=3$, for various $N$ at criticality and zero external field as a function of $p/u$. As soon as $N \gtrsim 10$, the large $N$ limit is attained.

correction.[41] One can see that both our and DE calculations fail to reproduce the analytical result (15% error within DE, 8% for this work). Most remarkably, the large $N$ results seem to be better predicted with both NPRG calculation than with the six-loop resummed perturbation calculation of Ref. 40; indeed, the latter clearly fails to predict the large $N$ behavior. We shall be back to the $1/N$ limit of our calculation in the last section of the paper. Finally, it is interesting to notice that all results present a peak in the value of $\eta$ around $N \sim 2-3$ (see Table I).

Let us now turn to the critical exponent $\nu$. Close to criticality, the effective renormalized mass at zero external field (which is the same for the transversal and longitudinal propagating modes in the symmetric phase) behaves as

$$m_{ren}^2(\rho=0) = \frac{V'(\rho=0)}{Z_\kappa} \simeq |r-r_c|^{2\nu} \quad (\kappa \ll u), \qquad (46)$$

where $r$ is the bare square mass and $r_c$ its value at criticality. We have performed numerical calculations close to criticality in order to determine the critical exponent $\nu$ for various values of $N$. The results can be seen in Table I, together with those coming from DE at NLO and the best estimates in the literature. Within both strategies of calculation, one gets almost the same results, for all values of $N$. As occurring with the critical exponent $\eta$, here, comparison of our results with those from DE at NLO depends on the regulator used. For example, for $N=1$, DE at NLO with the regulator of the present paper gives $\nu=0.625$,[38] $\nu=0.6307$ with the exponential regulator,[39] and $\nu=0.618$ with a power-law regulator.[22] Optimization makes a tiny difference.[38] In the present work, one gets 0.647 (strategy I) and 0.645 (strategy II). These numbers need to be compared with 0.630 12(16) (Ref. 3) and 0.630 20(12) (Ref. 6), from high-$T$ and MC calculations, respectively.

As for the large $N$ behavior, all calculations give the exact limit, $\nu=1$. In order to strengthen the study of this regime, it is convenient to plot the quantity $(1-\nu)N$, as we did in Fig. 4. Note that this quantity is prone to have much larger numerical error than $\nu$ as one moves to larger values of $N$. One can see that both DE at NLO and the present calculation fail to give the analytical large $N$ prediction for this quantity by not more than a few percent. On the other side, as was the case for the other critical exponent, six-loop calculation results from Ref. 40 suffer from bigger errors when comparing with the exact $1/N$ expansion. We shall be back to these points in the next section.

Besides these already very competitive results, the present method is fully devoted to calculate quantities that belong to a momentum regime where neither direct perturbation theory nor scaling properties can be used. These results are presented in the next section.

### B. Ultraviolet and crossover regimes

In Fig. 5, the physical self-energy at zero external field, $\Delta_A(p,\tilde{\rho}=0,\kappa\to 0)$, is plotted for various values of $N$. Notice that a simple dimensional analysis in Eq. (9) shows that the self-energy can be written as $\Delta_A(p,\tilde{\rho}=0,\kappa=0) = u^2\hat{\Delta}_A(p/u,\tilde{\rho}=0,\kappa=0)$, where $\hat{\Delta}_A$ is a dimensionless function of $p/u$. On the other hand, in the large $N$ limit, the critical self-energy is of order $1/N$ (see, e.g., the next section). As this limit is taken so that $uN$ is kept constant, the convenient function to plot is $N\Delta_A(p/(Nu),\tilde{\rho}=0,\kappa=0)/(Nu)^2$, which is shown in the figure. One can see that, as soon as $N$ reaches $\sim 10$, corrections to large $N$ behavior become small.

In the perturbative regime ($p \gg Nu$), one expects $\Gamma^{(2)}_{ab}(p) \sim [(N+2)/3]\delta_{ab}(u^2/96\pi^2)\log(p/u)$. In Ref. 36, it has been shown, for the $N=1$ case, that the analytical solution of Eq. (9) has this behavior, even though the coefficient in front of the logarithm, $u^2/9\pi^4$, is 8% larger (this coefficient is a two-loop quantity and the LO of the approximation method introduced in Ref. 34 does not include all the two-loop perturbative diagrams exactly). The analysis of Ref. 36 is generalizable for all $N$, provided we include the multiplicative factor $[(N+2)/3]\delta_{ab}$. Our approximate numerical solutions, within both methods, reproduce this result. As explained in Ref. 34, at the NLO of the present approximation scheme, which is beyond the scope of this paper, the contribution of the two-loop diagrams is completely included and the correct prefactor $[(N+2)u^2\delta_{ab}/288\pi^2]$ is recovered.

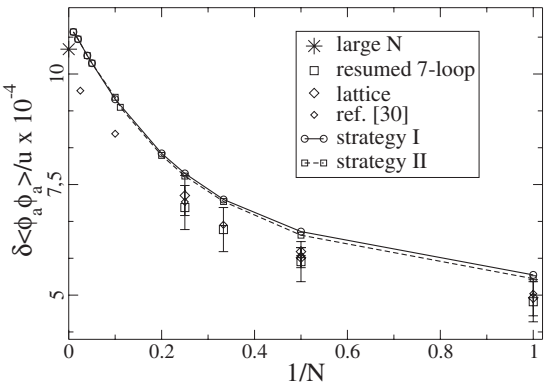


FIG. 6. $\delta\langle\phi_a\phi_a\rangle/u$ as a function of $1/N$.

For purposes of probing the intermediate momentum region between the IR and the UV, we have calculated the quantity

$$\frac{\delta\langle\phi_a\phi_a\rangle}{u} = \frac{1}{u}\int \frac{d^3p}{(2\pi)^3}\left(\frac{1}{p^2+\Delta_A(p)} - \frac{1}{p^2}\right), \qquad (47)$$

which is very sensitive to the crossover regime: The integrand in Eq. (47) is peaked at $p \sim (Nu)/10$.[28] In the $O(2)$ case and for $d=3$, this quantity determines the shift of the critical temperature of the weakly repulsive Bose gas.[25] It has thus been much studied recently using various methods, even for other values of $N$. In particular, the large $N$ limit for this quantity has been calculated analytically and found to be $1.05\times10^{-3}$.[47] As a consequence, $\delta\langle\phi_a\phi_a\rangle/u$ has been used as a benchmark for nonperturbative approximations in the $O(N)$ model.

In this work, we have found the values for $\delta\langle\phi_a\phi_a\rangle/u$ for some representative values of $N$ using both of the methods of approximation for the potential discussed in the previous section. The quantity we have chosen to calculate, $\delta\langle\phi_a\phi_a\rangle/u$, is the one having a finite large $N$ limit. The resulting curves are shown in Fig. 6, where they are compared with values obtained by lattice calculations,[42–44] resummed seven-loop calculations,[45,46] and to results obtained in Ref. 30. Those numbers, with their corresponding errors when available, are also presented in Table II. It can be seen that with our approximation strategy II, one gets slightly better results than with strategy I, but only for small enough $N$. For all values of $N$ where lattice and/or seven-loop resummed calculations exist, our results are almost within the error bars of those calculations, except for $N=2$, where very precise lattice results are available. In the large $N$ limit, one can see that our results differ from the exact value by less than 4%. Please note that the large $N$ behavior of $\delta\langle\phi_a\phi_a\rangle/u$ is given by $1/N$ corrections to the self-energy,[47] which are not calculated exactly at this level of approximation. Notice also that, within the two numerical strategies we use here, one gets the same large $N$ limit for $\delta\langle\phi_a\phi_a\rangle/u$. Both in the table and the figure, we also present results from Ref. 30, corresponding to an iterative *ad hoc* calculation within NPRG. These results correspond to an improved version of the NLO of that method, which was a precursor of the procedure presented in Ref. 34. It can be seen that, globally, these results are not significantly better than those from the present paper, corresponding to an approximate version of the method introduced in Ref. 34, at its LO.

In summary, when trying to calculate quantities in the momenta crossover region between the IR and the UV, the present approximation scheme seems to be particularly well suited: Already with approximated versions of the LO of the method, one gets numbers of about the same quality as those obtained with seven-loop resummed perturbation theory or lattice calculations.

## V. LARGE-$N$ BEHAVIOR

As shown in Ref. 34, the leading order of the approximating method introduced in that paper and used in the present one is exact in the large $N$ limit for any vertex function. This has been verified numerically in the previous section, where the correct large $N$ limits, $\eta=0$ and $\nu=1$, were extracted from the two-point function. In this section, in order to go beyond these results, we shall study the NLO of the $1/N$ expansion of the model to calculate both $\eta$ and $\nu$. The aim is to provide a test for the approximation in a situation where it

TABLE II. Summary of available results for the universal quantity $\delta\langle\phi_a\phi_a\rangle/u$. The analytically known exact large $N$ limit for this quantity is equal to $1.05\times10^{-3}$ (Ref. 47).

| $N$ | Lattice | Seven loops[a] | Ref. 30 | Strategy I | Strategy II |
|---|---|---|---|---|---|
| 1 | $(4.94\pm0.40)\times10^{-4}$ [b] | $(4.85\pm0.45)\times10^{-4}$ | $5.03\times10^{-4}$ | $5.44\times10^{-4}$ | $5.37\times10^{-4}$ |
| 2 | $(5.98\pm0.09)\times10^{-4}$ [c] | $(5.76\pm0.45)\times10^{-4}$ | $5.89\times10^{-4}$ | $6.44\times10^{-4}$ | $6.35\times10^{-4}$ |
| | $(5.85\pm0.22)\times10^{-4}$ [d] | | | | |
| 3 | | $(6.48\pm0.50)\times10^{-4}$ | $6.57\times10^{-4}$ | $7.18\times10^{-4}$ | $7.12\times10^{-4}$ |
| 4 | $(7.25\pm0.45)\times10^{-4}$ [b] | $6.98\pm0.50$ | $7.12\times10^{-4}$ | $7.75\times10^{-4}$ | $7.69\times10^{-4}$ |
| 10 | | | $8.66\times10^{-4}$ | $9.41\times10^{-4}$ | $9.47\times10^{-4}$ |
| 100 | | | | $1.10\times10^{-3}$ | $1.10\times10^{-3}$ |

[a]Reference 45.
[b]Reference 44.
[c]Reference 43.
[d]Reference 42.

is not exact, as well as to test the quality of the numerical calculations.

Before turning to this task, it is convenient to note that the large $N$ limit is taken so that $uN$ is constant and then $\Gamma_\kappa \sim O(N)$, $V_\kappa \sim O(N)$, $\Gamma_A \sim O(1)$, $\Gamma_B \sim O(1/N)$, and $\rho \sim O(N)$.[41] In Ref. 48, a generic form of the effective action in the large $N$ limit was found. Accordingly, a general parametrization of the two-point function in this limit is

$$\Gamma^{(2)}_{ab}(p,-p;\kappa;\phi) = [p^2 + V'_\kappa(\rho)]\delta_{ab} + \phi_a\phi_b\Gamma_B(p,-p;\rho), \tag{48}$$

where $\Gamma_B$ is the function defined in Eq. (11). Using this expression, it is possible to show that, within this limit, the flow equation for the potential at the leading order of DE [the local potential approximation (LPA)] is exact.[48] It has also been exploited to solve analytically the NPRG equations for any $n$-point function.[34] More precisely, doing the change of variables[49] $(\kappa,\rho)\to(\kappa,W)$, where

$$W = \frac{\partial V}{\partial \rho}, \tag{49}$$

it is possible to find the large $N$ limit for both the potential [or its inverse function $\rho=f(W)$] (Ref. 49) and $\Gamma_B$ (Ref. 34):

$$f_\kappa(W) = f_\Lambda(W) + \frac{N}{2}\int \frac{d^dq}{(2\pi)^d}\left\{\frac{1}{q^2+W+R_\Lambda(q^2)} - \frac{1}{q^2+W+R_\kappa(q^2)}\right\}, \tag{50}$$

$$\Gamma_B(p,-p;\rho) = \frac{u}{3}\left(1 + \frac{Nu}{6}\int \frac{d^dq}{(2\pi)^d}\frac{1}{q^2+W+R_\kappa(q^2)}\frac{1}{(q+p)^2+W+R_\kappa((q+p)^2)}\right)^{-1}, \tag{51}$$

which, in particular, enables for an explicit solution for the $f_\kappa$ function [in $d=3$ and for the regulator (30)]:

$$\rho = f_\kappa(W) = \frac{3}{u}W - \frac{3}{u}r_R + \frac{3}{2}K_dN\kappa - K_d\frac{N}{2}\frac{\kappa^3}{\kappa^2+W} + \frac{3}{2}NK_dWC(W), \tag{52}$$

where $r_R = r_\Lambda + K_dN\Lambda u/3$ and $C(W)$ is defined by

$$C(W) \equiv \int_\kappa^\infty dq \frac{1}{q^2+W} = \begin{cases} \dfrac{1}{\sqrt{W}}\left(\dfrac{\pi}{2} - \mathrm{Arctan}\left(\dfrac{\kappa}{\sqrt{W}}\right)\right) & (W>0) \\ \dfrac{1}{2\sqrt{-W}}\log\left(\dfrac{\sqrt{-W}+\kappa}{\sqrt{-W}-\kappa}\right) & (W<0). \end{cases}$$

Observe that $W \sim O(1)$.

### A. Critical exponent $\eta$

The procedure to calculate the critical exponent $\eta$ is given by Eqs. (A1)–(A6) of Appendix A. From the definitions in Eqs. (A1)–(A3), one can see that $\chi_A \sim O(1)$ and $\chi_B \sim O(1/N)$. As for the anomalous dimension, let us first observe that at leading order, $\chi_A(\tilde{\rho}) \equiv 1$ [see Eq. (48)]. Accordingly, $\chi'_A(\tilde{\rho}) \sim O(1/N^2)$. Thus, Eq. (A6) implies that $\eta \sim O(1/N)$. In order to find $\eta$, it is then necessary to get $\chi_B$ at its leading order [i.e., $O(1/N)$] and $\chi_A$ at its next-to-leading order (i.e., also $1/N$). The first function follows from Eq. (A2); expanding Eq. (51) to order $p^2$, one gets

$$Z_B = \frac{\frac{Nu^2}{18}K_3\left[\frac{1}{3}\frac{\kappa^3}{(\kappa^2+W)^3} + \frac{1}{4}\frac{\kappa}{(\kappa^2+W)^2} - \frac{1}{8W}\frac{\kappa}{\kappa^2+W} + \frac{1}{8W}C(W)\right]}{\left[1 + \frac{Nu}{6}K_3\left(\frac{\kappa^3}{(\kappa^2+W)^2} + \frac{3}{2}\frac{\kappa}{\kappa^2+W} + \frac{3}{2}C(W)\right)\right]^2}. \tag{53}$$

Finally, using Eq. (A3) and introducing the dimensionless quantities $\tilde{f}=f/(K_3\kappa)$, $w=W/\kappa^2$, and $\hat{u}=K_3u/\kappa$, the exact leading order expression for $\chi_B$ simply follows (remember that, for $N\to\infty$, $Z_\kappa=1$ and $\eta=0$).

We now turn to the next-to-leading order expression for $\chi_A$. In order to do so, we shall solve its flow equation, i.e., Eq. (A4), up to order $1/N$. One can then define

$$\chi_A = 1 + \frac{\hat{\chi}_A}{N}.$$

Introducing this expression in the flow equation (A4) and keeping only leading terms in $1/N$, one gets

$$\partial_t \hat{\chi}_A - (d-2)\tilde{\rho}\hat{\chi}_A' + \frac{N\hat{\chi}_A'}{(1+w)^2} = \eta N + \frac{8N\tilde{\rho}}{1+w+2\tilde{\rho}w'}\frac{\chi_B w'}{(1+w)^2} - \frac{2N\chi_B}{(1+w)^2} - \frac{4N\tilde{\rho}w'^2}{(1+w+2\tilde{\rho}w')^2(1+w)^2}. \tag{54}$$

Notice that, by construction, $\hat{\chi}_A \sim O(1)$ [and then $\hat{\chi}_A' \sim O(1/N)$]. Accordingly, in the right-hand side of Eq. (54), only the leading order expressions of both $\chi_B$ and $w$ are needed. They follow from Eqs. (52) and (53) after going to dimensionless variables.

Going to variables $(\kappa, w)$, using $\partial_t|_\rho = \partial_t|_w + \partial_\kappa w \partial_w$ and Eq. (A1), we end up with [where we define $\partial_w \tilde{f}_\kappa(w) \equiv \tilde{f}'_\kappa(w)$]

$$\partial_t \hat{\chi}_A(w) - 2w\partial_w \hat{\chi}_A(w) = \eta N + \frac{8N\tilde{f}(w)}{1+w+2\tilde{f}(w)/\tilde{f}'}\frac{\chi_B/\tilde{f}'(w)}{(1+w)^2} - \frac{2N\chi_B(w)}{(1+w)^2} - \frac{4N\tilde{f}/(\tilde{f}'(w))^2}{[1+w+2\tilde{f}(w)/\tilde{f}'(w)]^2(1+w)^2}. \tag{55}$$

Notice that it is convenient to work in the particular case $w=0$, i.e., at the minimum of the potential, where the equation is much simpler. Going to the IR fixed point, $\kappa\partial_\kappa \chi_A(w) \equiv 0$ (and, equivalently, $\hat{u} \to \infty$), it then follows that

$$\eta^* = \frac{1}{4N} + O\left(\frac{1}{N^2}\right). \tag{56}$$

One expects the calculation of $\eta^*$ to be independent of the renormalization point. However, once approximations are done, there is normally a small dependence on the precise renormalization point. In this case, though, observe that all over this calculation, we need not consider the specific renormalization condition introduced in Eqs. (29) and (32) (i.e., $\rho_0=0$). It then turns out that the obtained value of $N\eta^*$, when $N \to \infty$, does not depend on the chosen renormalization point.

The analytical value of $\eta^*$ obtained above is reproduced by our numerical results (see Fig. 3 and Table I). The exact value for the $1/N$ correction to $\eta^*$ in $O(N)$ models is known:[50] $8/(3\pi^2) \simeq 0.27$. It turns out that the error of our (both numerical and analytical) calculation turns out to be of about 8%, which is smaller than the error involved in both DE and six-loop resummed perturbative calculations (see Fig. 3).

A surprising fact is that the ratio between our result $(1/4)$ and the correct number $[8/(3\pi^2)]$ is exactly the same as the ratio between the correct result for the ultraviolet coefficient in front of the logarithm, $(N+2)u^2/(288\pi^2)$, and ours, $(N+2)u^2/(27\pi^4)$. It thus seems that, at least for $\eta$, the LO of the approximate procedure introduced in Ref. 34 misses the second order of the $1/N$ expansion by the same amount that it misses the second order of the perturbative expansion.

It is important to notice that the calculation presented above is valid for both of methods of approximation described in Sec. III of this paper. This is due to the fact that in this section we only needed the large $N$ limit of the potential, which is already exact in the case of the approximation used in strategy I.

### B. Critical exponent $\nu$

Let us now move on to the analysis of the $1/N$ correction for the behavior of the critical exponent $\nu$. We are dealing here with a critical point for a second order phase transition, with only one IR unstable direction under the RG flow. The exponent $\nu$ is related to the eigenvalue of the linearized flow in this relevant direction.

It will be useful to start with a study of the large $N$ limit for this quantity. Due to the significant simplification brought by working close to $w=0$ in the study of $\eta$ just presented, a similar strategy will now be adopted, defining

$$w = a(\tilde{\rho}-\rho_0) + \frac{b}{2}(\tilde{\rho}-\rho_0)^2 + O((\tilde{\rho}-\rho_0)^3),$$

with

$$w(\rho_0) = 0, \quad a = w'(\rho_0), \quad b = w''(\rho_0).$$

It is easy to find equations for this set of variables, which in the large $N$ limit decouple,[48] yielding the equations

$$\partial_t \rho_0 = -(d-2)\rho_0 + N, \tag{57}$$

$$\partial_t a = (d-4)a + 2Na^2, \tag{58}$$

$$\partial_t b = (2d-6)b + 6N(ab - a^3). \tag{59}$$

It is then possible to find the non-Gaussian fixed point value for these quantities in the large $N$ limit:

$$\rho_0^* = \frac{N}{d-2}, \tag{60}$$

$$a^* = \frac{4-d}{2N}, \tag{61}$$

$$b^* = \frac{6Na^{*3}}{2(d-3)+6Na^*} = \frac{3}{4N^2}\frac{(4-d)^3}{6-d}. \tag{62}$$

The flow equations for $\rho_0(t)$ and $a(t)$, Eqs. (57) and (58), can be solved analytically, yielding

$$\rho_0(t) = \rho_0^* + Pe^{-(d-2)t}, \tag{63}$$

$$a(t) = a^* \frac{1}{Ae^{(4-d)t}+1}. \tag{64}$$

These expressions, together with straightforward calculations for the behavior of $b(t)$ or any other higher order cou-

pling near the fixed point, clearly show that, in the large $N$ limit, the only unstable quantity under the RG flow, as $t \to -\infty$ ($\kappa \to 0$), is $\rho_0(t)$. This allows for the determination of the expected large $N$ critical exponent $\nu^{LO}=1/(d-2)$; in particular, $\nu=1$ for $d=3$.

Moving on to the analysis of the NLO in the $1/N$ expansion, we will from now on specialize to the simpler case of the first resolution strategy of Sec. III. Observe that results should not differ by much in the case of the improved strategy of Sec. III B, as the numerical calculations for both approximations seem to converge rapidly as $N$ increases.

The NLO flow equation for $\rho_0$, for the case of strategy I, is

$$\partial_t \rho_0 = -(d-2+\eta)\rho_0 + \left(1-\frac{\eta}{d+2}\right)\left[(N-1)+\frac{3+2\rho_0\frac{b}{a}}{(1+2\rho_0 a)^2}\right]. \tag{65}$$

Notice here that the functions $a(t)$ and $b(t)$ need only be known in their large $N$ limit. We will focus in solutions for this flow equations that are near the fixed point. We can then write, for the quantities in the right-hand side of Eq. (65),

$$\rho_0(t) = \rho_0^* + \epsilon\hat{\rho}_0 e^{-t(d-2)}, \tag{66}$$

$$b(t) = a^* + \epsilon\hat{a}(t), \tag{67}$$

$$b(t) = b^* + \epsilon\hat{b}(t), \tag{68}$$

$$\eta(t) = \eta^* + \epsilon\hat{\eta}\hat{\rho}_0 e^{-t(d-2)}, \tag{69}$$

where, for $\rho_0$ and $\hat{\eta}$, we are explicitly taking out the known large $Nt$ dependence, and in the case of $\hat{\eta}$, we are defining it with an ansatz to be justified later. As for the left-hand side of Eq. (65), we can, in principle, also write $\rho_0(t)=\rho_0^*+\epsilon\hat{\rho}_0^{(1)}\times(t)e^{-t(d-2)}$. Expanding Eq. (65) to order $\epsilon$, one can reach the expression [throwing away terms of order $(1/N)$]

$$\partial_t\hat{\rho}_0^{(1)}(t) = -\eta^*\hat{\rho}_0 - \hat{\eta}\rho_0^*\hat{\rho}_0 - \frac{\hat{\eta}N}{d+2}\hat{\rho}_0 + \left[\frac{2}{a^*}\left(\rho_0^*\hat{b}e^{t(d-2)} + \hat{\rho}_0 b^* - \rho_0^* b^*\frac{\hat{a}e^{t(d-2)}}{a^*}\right) - \frac{4\left(3+\frac{2}{a^*}\rho_0^* b^*\right)(\rho_0^*\hat{a}e^{[t(d-2)]}+\hat{\rho}_0 a^*)}{1+2\rho_0^* a^*}\right]\frac{1}{(1+2\rho_0^* a^*)^2}. \tag{70}$$

As already stated, we know that in the large $N$ limit, $\hat{a}(t)$ and $\hat{b}(t)$ go to zero after $t$ gets negative enough. Nonetheless, we cannot, in principle, assert the same for the behavior of $\eta$, and, in fact, we will show below that, as $\eta$ is already a quantity of order $O(1/N)$, the IR unstable direction of the flow has components in the linearized directions of both $\hat{\rho}_0$ and $\hat{\eta}$. If we consider $|t|$ large enough for $\hat{a}$ and $\hat{b}$ to be negligible, the following flow equation is found:

$$\frac{1}{\hat{\rho}_0}\partial_t\hat{\rho}_0^{(1)}(t) = -\eta^* - \hat{\eta}\rho_0^* - \frac{\hat{\eta}N}{d+2} + \left[\frac{2b^*}{a^*} - \frac{12a^*+8\rho_0^* b^*}{1+2\rho_0^* a^*}\right]\frac{1}{(1+2\rho_0^* a^*)^2}. \tag{71}$$

Knowing the large $N$ behavior for $\hat{\rho}_0^{(1)}(t)$ [see Eq. (70)], one can assume that, at NLO of the $1/N$ expansion,

$$\hat{\rho}_0^{(1)}(t) = \hat{\rho}_0 e^{(-ty_1/N)} \simeq \hat{\rho}_0\left(1 - t\frac{y_1}{N} + \cdots\right),$$

where, in $d=3$, it is easy to check that $y_1=-\nu^{(1)}$, i.e., the correction for $\nu$ at NLO in $1/N$ [$\nu=1/(d-2)+\nu^{(1)}/N$]. The equation for $\hat{\rho}_0^{(1)}$ can then be written as an equation for $\nu^{(1)}$,

$$\frac{\nu^{(1)}}{(d-2)^2 N} = -\eta^* - \hat{\eta}\rho_0^* - \frac{\hat{\eta}N}{d+2} - \left[\frac{2b^*}{a^*} - \frac{12a^*+8\rho_0^* b^*}{1+2\rho_0^* a^*}\right]\frac{1}{(1+2\rho_0^* a^*)^2}, \tag{72}$$

an expression which, when evaluated in $d=3$ using Eqs. (57), (61), and (62) and also Eq. (56) yields the relationship

$$\nu^{(1)} = -1 - \frac{6N\hat{\eta}}{5}. \tag{73}$$

The $-1$ in the last expression is the bulk of the required result, as $\hat{\eta}$ is expected to bring only a small contribution, which will be calculated in what follows.

Note before that the calculation so far presented is independent of the renormalization scheme, just as for the case of $\eta$ of the last section. In what follows, we will calculate the correction $\hat{\eta}$, which does depend on the point where the value of $\eta$ is fixed. Nevertheless, as stated in the last section, the numerical results found for the quantity $(1-\nu)N$ suffer from a quite large numerical error for large values of $N$. This makes impossible to distinguish the results between the two strategies presented in this paper, or between different renormalization schemes.

The starting point for the calculation of $\hat{\eta}$ is Eq. (55) for $\hat{\chi}_A(\tilde{\rho},t)$. In it, scheme dependence can only come from the running of $\eta_\kappa$ and from boundary conditions. When one considers the fixed point solution for $\hat{\chi}_A$, all the scheme dependence should come from the boundary conditions, as we have already shown that $\eta^*$, the fixed point solution for $\eta_\kappa$, is scheme independent. Therefore, the fixed point equation is of the form $w\partial_w\hat{\chi}_A = N\eta^* + F^*(w)$, where the right-hand side is scheme independent and thus the only consequence of the renormalization scheme on the fixed point solution is an additive constant.

Near the fixed point, in the right-hand side $F(w,t) = F^*(w) + \epsilon e^{-t(d-2)}\hat{F}(w)$, and similarly, $\hat{\chi}_A(w,t) = \hat{\chi}_A^*(w) + \epsilon e^{-t(d-2)}\tilde{\chi}_A$. At order $\epsilon$,

$$(d-2)\tilde{\chi}_A(w) + 2w\partial_w\tilde{\chi}_A(w) + N\hat{\eta} = -\tilde{F}(w). \tag{74}$$

Defining the variable $\bar{\chi}_A \equiv \tilde{\chi}_A + N\hat{\eta}/(d-2)$, it is straightforward to find the only solution to Eq. (74), which is a regular function for all values of $w$, and also turns out to be scheme independent,

$$\bar{\chi}_A(w) = -\frac{1}{2}|w|^{(2-d)/2}\int_0^w dw'|w'|^{(d-4)/2}\tilde{F}(w'). \tag{75}$$

As for the function $\tilde{F}(w)$, it is easily obtained by an order $\epsilon$ expansion of the function $F(w)$, taking into account that $(f')^* = (f^*)'$, and the fact that $\chi_B$ has a contractive IR behavior,

$$\begin{aligned}\tilde{F}(w) = \frac{-\hat{\rho}_0 N}{(1+w)^2}\Bigg\{ & \frac{8\chi_B^*(w)/(\tilde{f}^*)'(w)}{1+w+2\tilde{f}^*(w)/(\tilde{f}^*)'(w)} \\ & - \frac{16\tilde{f}^*\chi_B^*(w)/[(\tilde{f}^*)'(w)]^2}{[1+w+2\tilde{f}^*(w)/(\tilde{f}^*)'(w)]^2} \\ & - \frac{4}{[(f^*)'(w)]^2}\frac{1}{[1+w+2\tilde{f}^*(w)/(\tilde{f}^*)'(w)]^2} \\ & + \frac{16}{[(f^*)'(w)]^3}\frac{\tilde{f}^*(w)}{[1+w+2\tilde{f}^*(w)/(\tilde{f}^*)'(w)]^3}\Bigg\},\end{aligned} \tag{76}$$

where the factor $\hat{\rho}_0$ comes from the $t$ dependence of the function $\tilde{f}(w,t) = \tilde{f}^*(w) + \epsilon\hat{\rho}_0 e^{t(d-2)}$. Note that this factor justifies our initial ansatz for $\hat{\eta}$, Eq. (69).

After calculating the integral in Eq. (75), which can only be done numerically, one can impose the chosen renormalization prescription and obtain the numerical value of $\hat{\eta}$ which would complete the calculation of $\nu^{(1)}$. If we take the renormalization condition $\tilde{\chi}_A(w(\rho=0))=0$ used for the numerical results already presented, we find

$$\hat{\eta} = \frac{d-2}{N}\bar{\chi}_A(w^*(\rho=0)). \tag{77}$$

In $d=3$, numerical integration yields $\bar{\chi}_A(w^*(\rho=0)) \simeq 0.028\,238$, which allows for finding the NLO $1/N$ expansion correction for $\nu$ under our approximation scheme:

$$\nu \simeq 1 - \frac{1.034}{N}, \tag{78}$$

which is to be compared with the exact NLO $1/N$ expansion result[41] $\nu = 1 - 1.081/N$; in this case, then, the analytical error induced by the approximation used in this work is of the order of 5%, that is, less than that involved in the determination of $\eta$. Our numerical results seem to reproduce the analytical value given by Eq. (78), even though the numerical uncertainty for the quantity $N(1-\nu)$ grows for $N \to \infty$ (see Fig. 4).

As in the case of $\eta$, the results of this work seem to better reproduce the large $N$ behavior of the model when compared with DE or six-loop resummed perturbative calculations. In fact, as can be seen in Fig. 4, there appears to be a notorious disagreement between the expected large $N$ behavior and the resummed perturbative results of Ref. 40.

## VI. CONCLUSIONS AND PERSPECTIVES

In this paper, we calculate the two-point functions of the $O(N)$ model, in all ranges of momenta, i.e., either the IR, the UV, or the crossover intermediate region. We use a method proposed in Ref. 34, which allows for an approximate solution for any $n$-point function NPRG flow equation. Although this method can be systematically improved, in the present work, we consider only the leading order (LO) of this approximation procedure. In fact, in order to deal with a simpler numerical problem, on top of the already approximated flow equation, we have done extra assumptions to simplify the propagators. Moreover, we have tested two strategies: While the first one is simpler (we call it strategy I), it misses the two-loop exactness of the potential; within the second one (strategy II), which implies a small extra numerical effort, the two-loop expression is recovered. We have shown that both strategies can be justified; in addition, they are exact both perturbatively and in the large $N$ limit.

We have calculated various quantities to gauge the quality of the two-point function obtained within both strategies. In the IR regime, our solutions correctly reproduce the scaling properties. We have calculated two critical exponents, $\eta$ and $\nu$, for some representative values of $N$. We got numbers in reasonable agreement with the best known results available in the literature, obtained either with lattice or seven-loop resummed perturbative calculations. Within strategy II, our numbers turn out to be of the same quality of those obtained with derivative expansion (DE) at NLO. Notice, however, that DE is only well suited to reproduce these scaling quantities. When going to large values of $N$, our numerical results seem to reproduce the analytically known large $N$ limits, exactly at the LO and approximately at the NLO in the $1/N$ expansion. This also happens with DE results but not with those from a six-loop resummed perturbative calculation[40] (in fact, as soon as $N \gtrsim 5-10$, results from Ref. 40 seem to deviate from the correct large $N$ behavior).

The UV behavior of the $O(N)$ model two-point function is, of course, very well known: It presents a logarithmic shape, the precoefficient following from a two-loop calculation. One can analytically prove that the self-energy following from both our strategies does have this logarithmic shape. Nevertheless, as the LO of the approximate method of Ref. 34 does not exactly include all two-loop diagrams contributing to the two-point function, the precoefficient is missed by 8%. We have checked that our numerical results, within both methods, reproduce these analytical predictions.

The intermediate crossover region between IR and UV regimes is certainly the most challenging one. In order to check the quality of our two-point function, we have calculated a quantity which is particularly sensitive to this momentum regime. Of course, this number cannot be obtained with DE and only lattice or resummed perturbative calculations, as well as analytical large $N$ results, exist. In this case, our method is largely competitive with the best available

results, except for the $N=2$ case, where very precise lattice results are known. We miss the analytical large $N$ limit for this quantity by 4%; notice that the calculated quantity is of NLO in a $1/N$ expansion, which is not completely included in our approximate calculation.

Let us finally add a remark concerning our results: As expected, strategy II is more accurate than strategy I, but the differences get very small when going to large values of $N$. This is related to the fact that in the large $N$ limit, the approximate propagators we used in strategy I become exact.

Within the NPRG, two *ad hoc* calculations can be quoted here. First, in Ref. 27, an approximate solution of the flow equation including only a limited number of vertices could be calculated, but the result is unstable when trying to improve the method.[31] On the other side, in Refs. 28–30, an *ad hoc* method which can be considered as the precursor of the method presented in Ref. 34 is used to get a two-point function with all the expected properties; nevertheless, acceptable numbers only follow after an improved NLO order variation of the method and after a lengthy analytical and numerical effort.

We have also studied analytically the $1/N$ expansion of the critical exponents $\eta$ and $\nu$. In fact, as the first order in the expansion ($\eta=0$ and $\nu=1$) is trivially reproduced by our calculation, we went up to the second order. In the case of $\eta$, we found a result 8% smaller than the correct one. As for $\nu$, we get $(1-\nu)N=1.03+O(1/N^2)$, while the correct result is $(1-\nu)N=1.081+O(1/N^2)$. Here, we miss the correct result by only 5%. Finally, let us notice that our results seem to reproduce the expected analytical predictions. This is a strong support for our numerics.

To conclude, we observe that this approximate method to calculate two-point functions at finite momenta within the NPRG seems to work properly for all values of $N$. It reproduces, already at the LO, all the expected behavior of the self-energy, giving, in most of the regions of $N$ and $p$, results similar to those of the best accepted values in the literature. Moreover, in the large $N$ limit, one gets the best numbers, if comparing with DE or resummed six-loop calculations. The result of this paper thus extend and confirm those already obtained in Ref. 36 for the Ising universality class.

For the near future, two works are to be developed. As a natural extension, it would be interesting to go beyond strategies I and II and try to numerically solve the full approximate equation for the two-point function, Eq. (9). On the other side, all these works call for an application of this method to nonperturbative problems, as, e.g., QCD, where only approximate procedures including a limited number of vertices have been considered up to now.


## ACKNOWLEDGMENTS

We thank J. P. Blaizot, B. Delamotte, and H. Chate for useful discussions. The authors wish to acknowledge PEDECIBA.


## APPENDIX A: THE $p=0$ SECTOR

Within strategy I, one first solves the flow equations of the "$p=0$" sector, i.e., those for the potential $V_\kappa(\rho)$ and the field renormalization constant $Z_\kappa$ (see Sec. III). In fact, this is nothing but a variation of the local potential approximation (LPA), which includes a ($\rho$ independent) field renormalization constant.[16] Although this is a very well known procedure, its yields depend on the precise definition one uses for $Z_\kappa$. As discussed in the main text, in order to describe correctly the scaling regime, in our case, the flow equation for $Z_\kappa$ has to be compatible with the approximate Eq. (9) for the two-point function.

Let us first consider the flow equation for the potential. It follows from Eq. (21) with the $I^{(1)}$ functions given by the analytic expression from Eq. (31). In fact, it is numerically preferable to solve the flow equation for $w_\kappa(\tilde{\rho})=\partial_{\tilde{\rho}} v_\kappa(\tilde{\rho})$ which reads

$$\partial_t w_\kappa = -(2-\eta_\kappa)w_\kappa + (d-2+\eta_\kappa)\tilde{\rho} w'_\kappa - \left(1-\frac{\eta_\kappa}{d+2}\right) \times \left(\frac{(N-1)w'_\kappa}{(1+w_\kappa)^2} + \frac{3w'_\kappa + 2\tilde{\rho} w''_\kappa}{(1+w_\kappa+2\tilde{\rho} w'_\kappa)^2}\right).$$

As for $Z_\kappa$, let us first define

$$Z_A(\rho,\kappa) \equiv 1 + \left.\frac{\partial \Delta_A(p;\rho)}{\partial p^2}\right|_{p=0}, \tag{A1}$$

$$Z_B(\rho,\kappa) \equiv \left.\frac{\partial \Delta_B(p;\rho)}{\partial p^2}\right|_{p=0}, \tag{A2}$$

whose flow equations follow from those of $\Delta_A$ and $\Delta_B$. Then, one imposes the definition of $Z_\kappa$ given by Eq. (29). In fact, as the functions $Z_A(\rho,\kappa)$ and $Z_B(\rho,\kappa)$, as well as the potential, are zero momentum quantities, it is preferable to define the following dimensionless quantities [see Eq. (37)]:

$$\chi_A(\tilde{\rho}) \equiv \frac{Z_A(\rho)}{Z_\kappa}, \quad \chi_B(\tilde{\rho}) \equiv \frac{Z_B(\rho)}{\kappa^{4-d} Z_\kappa^2 K_d^{-1}}. \tag{A3}$$

The flow equations for $\chi_A$ and $\chi_B$ are then

$$\partial_t \chi_A = \eta\chi_A + (d-2+\eta)\tilde{\rho}\chi'_A + 2\left(1-\frac{\eta}{d+2}\right)\left[\frac{2\tilde{\rho}}{(1+w+2\tilde{\rho}w')^2}\frac{1}{1+w}(2\chi'_A w') + \frac{2\tilde{\rho}}{(1+w)^2}\frac{2\chi_B w'}{1+w+2\tilde{\rho}w'} - \frac{1}{2}\frac{1}{(1+w+2\tilde{\rho}w')^2}(\chi'_A + 2\tilde{\rho}\chi''_A) - \frac{1}{2}\frac{1}{(1+w)^2}[(N-1)\chi'_A + 2\chi_B]\right] - \frac{2\tilde{\rho}}{(1+w+2\tilde{\rho}w')^2}\frac{1}{(1+w)^2}2w'^2, \tag{A4}$$

$$\partial_t \chi_B = (d-2+2\eta)\chi_B + (d-2+\eta)\tilde{\rho}\chi_B' + 2\left(1-\frac{\eta}{d+2}\right)\left[\frac{2(N-1)}{(1+w)^3}\chi_B w' + \frac{1}{(1+w+2\tilde{\rho}w')^3}\{6\chi_A' w' + 12\chi_B w' + 4\tilde{\rho}(\chi_A' w'' + 3\chi_B' w' + 2\chi_B w'') + 8\tilde{\rho}^2\chi_B' w''\} - \frac{1}{(1+w+2\tilde{\rho}w')^2}\frac{2\chi_A' w'}{(1+w)} - \frac{1}{(1+w)^2}\frac{2\chi_B w'}{(1+w+2\tilde{\rho}w')} - \frac{1}{2}\frac{(N-1)}{(1+w)^2}\chi_B' - \frac{1}{2}\frac{1}{(1+w+2\tilde{\rho}w')^2}(5\chi_B' + 2\tilde{\rho}\chi_B'') + \left(\frac{1}{1+w+2\tilde{\rho}w'} + \frac{1}{1+w}\right)\frac{1}{1+w}\frac{\chi_B w'}{1+w+2\tilde{\rho}w'}\right] - (N-1)\frac{w'^2}{(1+w)^4} - \frac{1}{(1+w+2\tilde{\rho}w')^4}(9w'^2 + 12\tilde{\rho}w'w'' + 4\tilde{\rho}^2 w''^2) + \frac{1}{(1+w)^2}\frac{2w'^2}{(1+w+2\tilde{\rho}w')^2}. \tag{A5}$$

Finally, the value of $\eta_\kappa$ follows from Eq. (32):

$$\eta_\kappa = \frac{[N\chi_A'(\tilde{\rho}=0) + 2\chi_B(\tilde{\rho}=0)]}{[1+w(\tilde{\rho}=0)]^2 + \frac{[N\chi_A'(\tilde{\rho}=0) + 2\chi_B(\tilde{\rho}=0)]}{d+2}}. \tag{A6}$$

In strategy I, the $p=0$ sector of the theory thus follows from the simultaneous solution of the three flow equations, Eqs. (A1), (A4), and (A5), together with Eq. (A6). Equation (A1) is solved starting from the initial condition at $\kappa=\Lambda$:

$$w_\kappa(\tilde{\rho}, \kappa=\Lambda) = \hat{m}_\Lambda^2 + \hat{g}_\Lambda \tilde{\rho}. \tag{A7}$$

where the dimensionless parameters $\hat{m}_\Lambda$ and $\hat{g}_\Lambda$ are related to the parameters $r$ and $u$ of the classical action, Eq. (10), by ($d=3$)

$$\hat{m}_\Lambda^2 = \frac{r}{\Lambda^2}, \quad \hat{g}_\Lambda = \frac{u}{\Lambda}\frac{K_3}{3}. \tag{A8}$$

As for the initial conditions for the functions $\chi$, they follow from the definitions in Eqs. (A1), (A2), (22), and (23), together with Eq. (10):

$$\chi_A(\tilde{\rho}; \kappa=\Lambda) = 1, \quad \chi_B(\tilde{\rho}; \kappa=\Lambda) = 0. \tag{A9}$$

The parameter $r$ is adjusted in order to be at criticality at zero external field, i.e., in order to have a vanishing physical mass. This is achieved imposing the dimensionless mass $m_\kappa^2(\tilde{\rho}=0) = w_\kappa(\tilde{\rho}=0)$ to reach a finite value when $\kappa \ll u$.

## APPENDIX B: THE FUNCTION $J$

In this section, we present the expressions for the function $J_d^{(3)}(p;\rho;\kappa)$ defined in Eq. (18). Using the approximate propagators from Eqs. (27), (28), (35), and (36), the integral can be done analytically (in $d=3$). One gets (see Ref. 36 for the $N=1$ case) the following.

(a) $\bar{p} > 2$, $\hat{m}_\beta^2 < 0$,

$$J_{3,\alpha\beta}^{(3)}(p;\kappa;\tilde{\rho}) = \frac{1}{\kappa Z_\kappa^2 (2\pi)^2}\frac{1}{(1+\hat{m}_\alpha^2)^2}\left\{2 + \frac{\eta}{2}\left(-\frac{5}{3} + \bar{p}^2 - 3\hat{m}_\beta^2\right) + \frac{1}{2\bar{p}}\left[-1 + \frac{\eta}{4} + (\bar{p} + \sqrt{-\hat{m}_\beta^2})^2\left(1 - \frac{\eta}{2} + \frac{\eta}{4}(\bar{p} + \sqrt{-\hat{m}_\beta^2})^2\right)\right]\log\left(\frac{\bar{p}-1+\sqrt{-\hat{m}_\beta^2}}{\bar{p}+1+\sqrt{-\hat{m}_\beta^2}}\right) + \frac{1}{2\bar{p}}\left[-1 + \frac{\eta}{4} + (\bar{p} - \sqrt{-\hat{m}_\beta^2})^2\left(1 - \frac{\eta}{2} + \frac{\eta}{4}(\bar{p} - \sqrt{-\hat{m}_\beta^2})^2\right)\right]\log\left(\frac{\bar{p}-1-\sqrt{-\hat{m}_\beta^2}}{\bar{p}+1-\sqrt{-\hat{m}_\beta^2}}\right)\right\} = \frac{1}{\kappa Z_\kappa^2 (2\pi)^2}\frac{2}{(1+\hat{m}_\alpha^2)^2}\left\{\frac{4}{\bar{p}^2}\left(\frac{1}{3} - \frac{\eta}{15}\right) + \frac{4}{\bar{p}^4}\left(\frac{1}{15} - \frac{\eta}{105} - \frac{\hat{m}_\beta^2}{3} + \frac{\eta\hat{m}_\beta^2}{15}\right) + \mathcal{O}(1/(\bar{p}^6))\right\}. \tag{B1}$$

(b) $\bar{p} \leqslant 2$, $\hat{m}_\beta^2 < 0$,

$$J^{(3)}_{3,\alpha\beta}(p;\kappa;\tilde{\rho}) = \frac{1}{\kappa Z_\kappa^2 (2\pi)^2}\frac{1}{(1+\hat{m}_\alpha^2)^2}\left\{-1+\frac{\eta}{4}+\frac{\eta\hat{m}_\beta^2}{4}+\bar{p}\left(\frac{3}{2}-\frac{\eta}{8}-\frac{7\eta\hat{m}_\beta^2}{8}\right)-\frac{3\eta}{4}\bar{p}^2+\frac{25\eta}{48}\bar{p}^3+\frac{1}{1+\hat{m}_\beta^2}\left[\frac{4}{3}-\frac{4\eta}{15}-\bar{p}+\frac{\eta}{3}\bar{p}^2+\left(\frac{1}{12}-\frac{\eta}{6}\right)\bar{p}^3+\frac{\eta}{120}\bar{p}^5\right]+\frac{1}{2\bar{p}}\left[1-\frac{\eta}{4}-(\bar{p}+\sqrt{-\hat{m}_\beta^2})^2\left(1-\frac{\eta}{2}+\frac{\eta}{4}(\bar{p}+\sqrt{-\hat{m}_\beta^2})^2\right)\right]\log\left(\frac{\bar{p}+1+\sqrt{-\hat{m}_\beta^2}}{1+\sqrt{-\hat{m}_\beta^2}}\right)+\frac{1}{2\bar{p}}\left[1-\frac{\eta}{4}-(\bar{p}-\sqrt{-\hat{m}_\beta^2})^2\left(1-\frac{\eta}{2}+\frac{\eta}{4}(\bar{p}-\sqrt{-\hat{m}_\beta^2})^2\right)\right]\log\left(\frac{\bar{p}+1-\sqrt{-\hat{m}_\beta^2}}{1-\sqrt{-\hat{m}_\beta^2}}\right)\right\} = \frac{1}{\kappa Z_\kappa^2 (2\pi)^2}\frac{1}{(1+\hat{m}_\alpha^2)^2}\left\{\frac{4}{3(1+\hat{m}_\beta^2)}\left(1-\frac{\eta}{5}\right)-\frac{2}{3(1+\hat{m}_\beta^2)^2}\bar{p}^2+\frac{2+\eta-2\hat{m}_\beta^2+\eta\hat{m}_\beta^2}{6(1+\hat{m}_\beta^2)^3}\bar{p}^3-\frac{2(1+\eta-5\hat{m}_\beta^2+\eta\hat{m}_\beta^2)}{15(1+\hat{m}_\beta^2)^4}\bar{p}^4+\mathcal{O}(\bar{p}^5)\right\}. \tag{B2}$$

(c) $\bar{p}>2$, $m_\beta^2 \geqslant 0$,

$$J^{(3)}_{3,\alpha\beta}(p;\kappa;\tilde{\rho}) = \frac{1}{\kappa Z_\kappa^2 (2\pi)^2}\frac{1}{(1+\hat{m}_\alpha^2)^2}\left(2+\frac{\eta}{2}\left(-\frac{5}{3}+\bar{p}^2-3\hat{m}_\beta^2\right)+\frac{1}{\bar{p}}\left\{\left[-1+\frac{\eta}{4}+(\bar{p}^2-\hat{m}_\kappa^2)\left(1-\frac{\eta}{2}+\frac{\eta}{4}(\bar{p}^2-\hat{m}_\beta^2)\right)-\eta\hat{m}_\beta^2\bar{p}^2\right]\frac{1}{2}\log\left(\frac{(\bar{p}-1)^2+\hat{m}_\kappa^2}{(\bar{p}+1)^2+\hat{m}_\kappa^2}\right)-2\hat{m}_\beta\bar{p}\left(1-\frac{\eta}{2}+\frac{\eta}{2}(\bar{p}^2-\hat{m}_\beta^2)\right)\left[\mathrm{Arctan}\left(\frac{\hat{m}_\beta}{\bar{p}-1}\right)-\mathrm{Arctan}\left(\frac{\hat{m}_\beta}{\bar{p}+1}\right)\right]\right\}\right) = \frac{1}{\kappa Z_\kappa^2 (2\pi)^2}\frac{1}{(1+\hat{m}_\alpha^2)^2}\left\{\frac{4}{\bar{p}^2}\left(\frac{1}{3}-\frac{\eta}{15}\right)+\frac{1}{105\bar{p}^4}[7-35\hat{m}_\beta^2+\eta(-1+7\hat{m}_\beta^2)]+\mathcal{O}(1/(\bar{p}^6))\right\}. \tag{B3}$$

(d) $\bar{p}\leqslant 2$, $m_\beta^2 \geqslant 0$,

$$J^{(3)}_{3,\alpha\beta}(p;\kappa;\tilde{\rho}) = \frac{1}{\kappa Z_\kappa^2 (2\pi)^2(1+\hat{m}_\alpha^2)^2}\left(-1+\frac{\eta}{4}+\frac{\eta\hat{m}_\beta^2}{4}+\bar{p}\left(\frac{3}{2}-\frac{\eta}{8}-\frac{7\eta\hat{m}_\beta^2}{8}\right)-\frac{3\eta\bar{p}^2}{4}+\frac{25\eta\bar{p}^3}{48}+\frac{1}{1+\hat{m}_\beta^2}\left(\frac{4}{3}-\frac{4\eta}{15}-\bar{p}+\frac{\eta\bar{p}^2}{3}+\frac{\bar{p}^3}{12}-\frac{\eta\bar{p}^3}{6}+\frac{\eta\bar{p}^5}{120}\right)+\frac{1}{\bar{p}}\left\{\left[1-\frac{\eta}{4}-(\bar{p}^2-\hat{m}_\beta^2)\left(1-\frac{\eta}{2}+\frac{\eta}{4}(\bar{p}^2-\hat{m}_\beta^2)\right)+\eta\hat{m}_\beta^2\bar{p}^2\right]\frac{1}{2}\log\left(\frac{(\bar{p}+1)^2+\hat{m}_\beta^2}{1+\hat{m}_\beta^2}\right)+2\hat{m}_\beta\bar{p}\left(1-\frac{\eta}{2}+\frac{\eta}{2}(\bar{p}^2-\hat{m}_\beta^2)\right)\left[\mathrm{Arctan}\left(\frac{\hat{m}_\beta}{\bar{p}+1}\right)-\mathrm{Arctan}(\hat{m}_\beta)\right]\right\}\right) = \frac{1}{\kappa Z_\kappa^2 (2\pi)^2(1+\hat{m}_\alpha^2)^2}\left\{\frac{4}{3(1+\hat{m}_\beta^2)}\left(1-\frac{\eta}{5}\right)-\frac{2}{3(1+\hat{m}_\beta^2)^2}\bar{p}^2+\frac{2+\eta-2\hat{m}_\beta^2+\eta\hat{m}_\beta^2}{6(1+\hat{m}_\beta^2)^3}\bar{p}^3-\frac{2(1+\eta-5\hat{m}_\beta^2+\eta\hat{m}_\beta^2)}{15(1+\hat{m}_\beta^2)^4}\bar{p}^4+\mathcal{O}(\bar{p}^5)\right\}. \tag{B4}$$

Finally, going to dimensionless variables, one can define

$$\tilde{J}_{\alpha\beta}(\tilde{p};\tilde{\rho}) \equiv J_{\alpha\beta}(p;\rho)\frac{\kappa Z_\kappa^2}{K_3}. \tag{B5}$$

*federico@fisica.edu.uy
†mendezg@fing.edu.uy
‡nicws@fing.edu.uy

[1] R. Guida and J. Zinn-Justin, J. Phys. A **31**, 8103 (1998).
[2] A. Butti and F. Parisen Toldin, Nucl. Phys. B **704**, 527 (2005).
[3] M. Campostrini, A. Pelissetto, P. Rossi, and E. Vicari, Phys. Rev. E **65**, 066127 (2002).
[4] M. Campostrini, M. Hasenbusch, A. Pelissetto, and E. Vicari, Phys. Rev. B **74**, 144506 (2006).
[5] M. Campostrini, M. Hasenbusch, A. Pelissetto, P. Rossi, and E. Vicari, Phys. Rev. B **65**, 144520 (2002).
[6] Y. Deng and H. W. J. Blote, Phys. Rev. E **68**, 036125 (2003).
[7] M. Hasenbusch, J. Phys. A **34**, 8221 (2001).
[8] M. Hasenbusch, A. Pelissetto, and E. Vicari, Phys. Rev. B **72**, 014532 (2005).
[9] A. Pelissetto and E. Vicari, Phys. Rep. **368**, 549 (2002).
[10] C. Wetterich, Phys. Lett. B **301**, 90 (1993).
[11] U. Ellwanger, Z. Phys. C **58**, 619 (1993).
[12] N. Tetradis and C. Wetterich, Nucl. Phys. B **422**, 541 (1994).
[13] T. R. Morris, Int. J. Mod. Phys. A **9**, 2411 (1994).
[14] T. R. Morris, Phys. Lett. B **329**, 241 (1994).
[15] C. Bagnuls and C. Bervillier, Phys. Rep. **348**, 91 (2001).
[16] J. Berges, N. Tetradis, and C. Wetterich, Phys. Rep. **363**, 223 (2002).
[17] B. Delamotte, D. Mouhanna, and M. Tissier, Phys. Rev. B **69**, 134413 (2004).
[18] B. Delamotte and L. Canet, Condens. Matter Phys. **8**, 163 (2005).
[19] D. Litim, Phys. Lett. B **486**, 92 (2000); D. F. Litim, Phys. Rev. D

**64**, 105007 (2001); Nucl. Phys. B **631**, 128 (2002); Int. J. Mod. Phys. A **16**, 2081 (2001).
[20] G. v. Gersdorff and C. Wetterich, Phys. Rev. B **64**, 054513 (2001).
[21] J. Berges, N. Tetradis, and C. Wetterich, Phys. Rev. Lett. **77**, 873 (1996).
[22] T. R. Morris and M. D. Turner, Nucl. Phys. B **509**, 637 (1998).
[23] T. Gollisch and C. Wetterich, Phys. Rev. B **65**, 134506 (2002).
[24] L. Canet, B. Delamotte, D. Mouhanna, and J. Vidal, Phys. Rev. B **68**, 064421 (2003).
[25] G. Baym, J. P. Blaizot, M. Holzmann, F. Laloe, and D. Vautherin, Phys. Rev. Lett. **83**, 1703 (1999).
[26] S. Weinberg, Phys. Rev. D **8**, 3497 (1973).
[27] S. Ledowski, N. Hasselmann, and P. Kopietz, Phys. Rev. A **69**, 061601(R) (2004).
[28] J. P. Blaizot, R. Mendez Galain, and N. Wschebor, Europhys. Lett. **72**, 705 (2005).
[29] J. P. Blaizot, R. Mendez-Galain, and N. Wschebor, Phys. Rev. E **74**, 051116 (2006).
[30] J. P. Blaizot, R. Mendez-Galain, and N. Wschebor, Phys. Rev. E **74**, 051117 (2006).
[31] N. Hasselmann, S. Ledowski, and P. Kopietz, Phys. Rev. A **70**, 063621 (2004).
[32] J. Cato, arXiv:hep-th/0401068 (unpublished); C. S. Fischer and H. Gies, J. High Energy Phys. 10 (2004), 0418.
[33] U. Ellwanger, Z. Phys. C **62**, 503 (1994); U. Ellwanger and C. Wetterich, Nucl. Phys. B **423**, 137 (1994); U. Ellwanger, M. Hirsch, and A. Weber, Eur. Phys. J. C **1**, 563 (1998); J. M. Pawlowski, D. F. Litim, S. Nedelko, and L. von Smekal, Phys. Rev. Lett. **93** 152002 (2004).
[34] J. P. Blaizot, R. Mendez Galain, and N. Wschebor, Phys. Lett. B **632**, 571 (2006).
[35] D. Guerra, R. Mendez-Galain, and N. Wschebor, Eur. Phys. J. B **59**, 357 (2007).
[36] J. P. Blaizot, R. Mendez-Galain, and N. Wschebor, Eur. Phys. J. B **58**, 297 (2007).
[37] Ulrich Ellwanger, Z. Phys. C **62**, 503 (1994).
[38] L. Canet, B. Delamotte, D. Mouhanna, and J. Vidal, Phys. Rev. D **67**, 065004 (2003).
[39] G. v. Gersdorff and C. Wetterich, Phys. Rev. B **64**, 054513 (2001).
[40] S. A. Antonenko and A. I. Sokolov, Phys. Rev. E **51**, 1894 (1995).
[41] M. Moshe and J. Zinn-Justin, Phys. Rep. **385**, 69 (2003).
[42] V. A. Kashurnikov, N. V. Prokof'ev, and B. V. Svistunov, Phys. Rev. Lett. **87**, 120402 (2001).
[43] P. Arnold and G. Moore, Phys. Rev. Lett. **87**, 120401 (2001).
[44] X. Sun, Phys. Rev. E **67**, 066702 (2003).
[45] B. M. Kastening, Phys. Rev. A **69**, 043613 (2004).
[46] J. L. Kneur, A. Neveu, and M. B. Pinto, Phys. Rev. A **69**, 053624 (2004).
[47] G. Baym, J.-P. Blaizot, and J. Zinn-Justin, Europhys. Lett. **49**, 150 (2000).
[48] M. D'Attanasio and T. R. Morris, Phys. Lett. B **409**, 363 (1997).
[49] N. Tetradis and D. F. Litim, Nucl. Phys. B **464**, 492 (1996).
[50] J. Zinn-Justin, *Quantum Field Theory and Critical Phenomena*, Fourth Ed. (Clarendon Press, Oxford, 2002).